Sedimentologika

Research article

Size and shape of carbonate grains: A comparison of measurement techniques

Chibuzor David Nworie*, Zane R. Jobe

Department of Geology and Geological Engineering, Colorado School of Mines, 1500 Illinois Street, Golden, CO, USA

*corresponding author: Chibuzor David Nworie (chibuzordavid3@gmail.com)

doi: 10.57035/journals/sdk.2025.e31.1742

Editors: Stéphane Bodin and Siddhi Joshi
Reviewers: Fares Azzam and one anonymous reviewer
Copyediting, layout and production: Jarred C. LLyod, Sara Biddle, Romain Vaucher and Marine Prieur

Submitted: 29.11.2024
Accepted: 15.09.2025
Published: 31.10.2025

Abstract | Grain size and shape significantly influence sediment transport and deposition, so accurate characterization is essential for understanding depositional dynamics. Biogenic carbonate grains, such as skeletal fragments, exhibit irregular morphologies that challenge traditional, single-diameter-based size estimates. To better characterize these non-spherical grains, two- or three-dimensional analyses are required. Micro-computed tomography (micro-CT) offers high-resolution, three-dimensional models of individual grains, enabling accurate quantification of volume, projection area, and shape. However, the high cost and limited accessibility of micro-CT in standard sedimentology labs hinder its widespread use. This study compares caliper measurements, sieve analysis, static image analysis (SIA), and dynamic image analysis (DIA) against a micro-CT reference dataset for sand-sized skeletal carbonate grains. We assess the accuracy of each method in capturing key grain properties relevant for hydrodynamic and geomechanical modeling, including volume, maximum projection area, nominal diameter, and Corey shape factor. We also evaluate the potential of predicting a grain's third dimension based on its maximum projection dimension, as measured through SIA of loose grains and thin sections. A regression model comparing SIA to known micro-CT values yields 72–78% accuracy. Results show that methods relying on axial dimensions systematically overestimate volume and maximum projection area. DIA tends to oversimplify grains as spherical, while SIA on thin sections may underestimate grain size due to slicing orientation effects. This study highlights the advantages and limitations of various measurement techniques and underscores the importance of selecting appropriate grain measurement techniques in sedimentological research.

Lay summary | Sediment grains are present in various natural depositional and anthropogenic environments and engineering structures. These grains often have irregular shapes, making it difficult to measure their size and shape accurately using traditional methods. While micro-computed tomography (micro-CT) can capture precise 3D models of individual grains, it is expensive and not widely accessible. This study compares the accuracy of more accessible measurement techniques, including caliper measurements and both static and dynamic image analysis, against micro-CT as the reference standard. The implications of accurate grain dimensions are far-reaching because they impact the prediction of the movement of sediment in natural and artificial flows. Such hydrodynamic distribution governs depositional-process dynamics that are crucial for reconstructing sediment dispersal patterns in nature and engineering projects. Our results indicate that most methods mis-estimate volume and maximum projection area, particularly for more complex shapes, whereas micro-CT provides the most accurate measurement of carbonate grains. Based on these findings, a possible method is proposed for obtaining the three-dimensional grain size and shape properties from two-dimensional projection measurements where limited information is available.

Keywords: Carbonate grains; Micro-CT; Volume–area relationships; Image analysis; Particle-size analysis.

1. Introduction

Sedimentary deposits in natural environments and engineered structures are composed of grains (i.e., particles) of mixed sizes and shapes. Sediment mobility depends on these grain properties (Krumbein, 1942; Yordanova and Hohenegger, 2007). Hence, quantification of grain dimensions is crucial for understanding sediment transport dynamics in depositional systems (Folk & Robles, 1964; Pilkey et al., 1967; Maiklem, 1968; Mulder & Alexander, 2001; Hawie et al., 2019; Cassel et al., 2021), as well as in the assessment of material properties in engineering applications (Walsh, 1988; Ghoddousi et al., 2014). For example, the hydrodynamic behavior of sediment grains and the depositional character of sediment accumulations rely on the accurate description of the interaction between grain characteristics (e.g., size, shape, density) and fluid properties (e.g., flow velocity, viscosity, flow confinement) (Stokes, 1851; Maiklem, 1968; Stingham et al., 1969; see De Kruijf et al., 2021 for review). In addition, the quality of subsurface reservoirs, relevant for the exploitation of aquifers, hydrothermal and petroleum accumulations, as well as carbon and hydrogen storage potential, depends on the distribution of sediment-grain properties (e.g., Worden et al., 2018).

Sediment grains are traditionally modeled as spheres (Stokes, 1851; Clift & Gauvin, 1971) or ellipsoids (Krumbein, 1942; Komar and Reimers, 1978; Baba and Komar, 1981; Smith and Cheung, 2003; Blott and Pye, 2008), which may be appropriate if sediment is composed of equant grains, such as siliciclastic grains that have undergone significant abrasion during transport (Maiklem, 1968; Braithwaite, 1973). Other sediment types like carbonates and volcanics are typically composed of irregular grains, which may be flat or elongated and may contain sharp grain corners, and for which a spherical grain model is inadequate (Bagheri et al., 2015, Sun et al., 2017). Irregular grain shapes influence the hydrodynamic behavior of sediments, in addition to density and shape variation (Folk & Robles, 1964; Pilkey et al., 1967; Yordanova & Hohenegger, 2007; Ford & Kench, 2012; De Kruijf et al., 2021). Density is particularly complex in skeletal carbonate grains due to intricate internal structures, such as chambers and micro-porosities, which modify the grain density (De Kruijf et al., 2021). This study focuses on the influence of grain shape and does not extend to the effects of density variability.

Various grain-shape descriptors have been proposed, commonly based on the ratios between grain axes to describe grain form (e.g., Clark, 1981; Le Roux, 1997; Blott and Pye, 2008; Wang et al., 2018; Riazi and Türker, 2019; De Kruijf et al., 2021). These axes may be treated as either mutually perpendicular or not, depending on the method used (Blott and Pye, 2008; Bagheri et al., 2015). However, the complexity of irregular sediment grains is insufficiently captured by these first-order descriptors of grain form (Griffiths, 1967; Barrett, 1980), necessitating the introduction of higher-order shape parameters that address the roundness of grain corners (Bowman et al., 2001; Oakey et al., 2005), and surface texture (Pettijohn, 1957).

Common techniques for the measurement of grain size, and in some cases also grain shape, include sieve analysis (Komar & Cui, 1984), caliper measurements (Blott and Pye, 2008; Bagheri et al., 2015), static image analysis (Al-Rousan, 2004; Al-Rousan et al., 2007; Buscombe et al., 2010), dynamic image analysis (Patchigolla and Wilkinson, 2009; Van Hateren et al., 2020; Buckland et al., 2021; Zhang et al., 2021), and micro-computerized tomography (i.e., micro-CT; Carlson et al., 2003; Cnudde and Boone, 2013; Maroof et al., 2020; Payton et al., 2022, 2024; Slootman et al., 2023; Houghton et al., 2024). Each of these methods has advantages and disadvantages: some techniques are laborious, time-consuming, computationally expensive, subjective in nature, or limited in their ability to differentiate among aggregate characteristics (see review in De Kruijf et al., 2021). The most accurate technique for characterizing sediment size and shape is arguably the acquisition of high-resolution grain models using micro-CT, from which detailed grain size and shape descriptors can be obtained. However, micro-CT analysis is more costly, data-intensive, and labor-intensive compared to other methods and is not commonly available in standard sedimentology laboratories.

The intricacies of grain-size and grain-shape determination are particularly relevant for biogenic carbonate sediments produced in tropical and cool-water carbonate environments (e.g., Schlager, 2003; Reijmer, 2021), comprising a major part of the world's modern and ancient ocean floors (Knowlton et al., 2010; Laugié, et al., 2019). Transported carbonates have gained increasing attention over the past decades (e.g., Jorry et al., 2006; Payros and Pujalte, 2008; Playton et al., 2010, 2018; Reijmer et al., 2012; Slootman et al., 2023). While recent studies have provided valuable insights into carbonate grain density and 3D morphology distribution (e.g., Slootman et al., 2023), many aspects of how grain properties influence transport dynamics remain insufficiently constrained. Biogenic carbonates are composed of skeletal remains that may exhibit a diverse range of forms and growth structures adopted by producing organisms, such as ribs and protrusions (Figure 1A-D) (Maiklem, 1968; Braithwaite, 1973). The irregular characteristics of carbonate sediments distort grain-size distributions when using sieve-based analysis, or other spherical-based methods that sort grains by their intermediate diameter (Braithwaite, 1973; Kench and McLean, 1996; Blott and Pye, 2008; Cuttler et al., 2017; Flemming, 2017).

Errors introduced by ignoring shape characteristics have implications for hydrodynamic predictions (Bagheri and Bonadonna, 2016; Riazi et al., 2020). Shape-dependent settling velocities are essential for accurate models of sediment transport dynamics in carbonate systems that play a critical role in understanding platform-to-basin source-to-sink processes (Jorry et al., 2006; Le Goff et al., 2021; Slootman et al., 2023). These dynamics are particularly valuable for reconstructing depositional patterns of sediment dispersal in carbonate environments (Morgan & Kench, 2014, 2016; Reijmer, 2021). Accurate sediment shape and size characterization is also essential for geomechanical properties (Askaripour et al., 2022), as well as for hazard assessment in marine engineering and slope stability analysis (Murff, 1987; Hohenegger, 2006; Lokier and Fiorini, 2016; Mohr et al., 2016; Shen et al., 2019). Thus, there is a need for accurate, rapid, and inexpensive methodologies available in standard sedimentology labs for the characterization of sediment grain size and shape.

This study evaluates the accuracy of four simple and inexpensive methods that are commonly available in most sedimentology laboratories for determining grain size and shape: (i) caliper measurement, (ii) static image analysis of loose grains, (iii) static image analysis of thin sections, and (iv) dynamic image analysis. The sediments analyzed consist of irregular, sand-sized grains of skeletal carbonate composition. Results from each method are compared against a reference dataset generated from micro-computed tomography (micro-CT) scans of the same sediment population, which serves as the closest approximation of the true grain dimensions. In addition, the micro-CT dataset is used to develop a regression model to predict the third dimension of irregular grains using two-dimensional measurements from the other methods. This model enables more robust estimation of 3D grain properties using standard, inexpensive methods available in any sedimentology lab.

2. Grain size and shape descriptors

Sediment grain dimensions are the principal parameters to characterize grain size and shape. The most common method for describing grain size is with a single diameter, such as the intermediate or sieve diameter used in the Wentworth (1922) scale (see also Krumbein 1941a, b). This model suffices for spheroidal grains but falls short for more ellipsoidal grains, for which models with three perpendicular axes are employed instead (Oakey et al., 2005; Blott and Pye, 2008). This approach offers a representation of grain size and shape using a bounding-box ellipsoid model (Krumbein 1941a, 1941b; Blott and Pye, 2008; Bagheri et al., 2015) that approximates a non-spherical grain based on three orthogonal axes: D_l (longest), D_i (intermediate), and D_s (shortest) (Figure 1). However, rather than three axial values, a single grain-size descriptor is useful and easier for quantitative comparison in statistical analysis. The actual volume of the grain can be recalculated into the diameter of a sphere with the same volume as the grain, the so-called equivalent diameter: $D_{eq} = \sqrt[3]{\frac{6}{\pi}.V_{measured}}$ (Gibbs et al., 1971). Since the actual volume is typically not measured, the bounding-box ellipsoid is often used as an approximation, the size of which can be condensed into the nominal diameter based on the volume of the ellipsoid: $D_n = \sqrt[3]{D_l.D_i.D_s}$.

Two-dimensional ratios can be computed from the three main grain axes as first-order shape descriptors (i.e., dealing with grain form; Griffiths, 1967; Barret, 1980), including flatness, elongation, and equancy (Blott and Pye, 2008). Flatness (D_s/D_i) quantifies platiness, providing insights into the planar attributes of grain shape. Elongation (D_i/D_l) describes how stretched a grain is in one direction to identify rod and blade shapes. Equancy (D_s/D_l) assesses the degree of uniformity in grain dimensions (Table 1). These ratios are the basis for the Zingg (1935) form classification that partitions four qualitative end-members: equants/spheroids, plates/discs, rods, and blades (Figure 1E-F). A quantitative approach is offered by the Corey (1949) shape factor (CSF), which is commonly used to parameterize grain shape with a single parameter: $CSF = D_s/\sqrt{D_i.D_l}$ (Table 1). CSF has a maximum value of one for spherical grains and decreases as grains become more ellipsoidal. However, CSF is unable to discriminate between the shapes in the Zingg classification (see CSF-isolines in Figure 1E-F).

The first-order dimensions that control the hydrodynamic properties of a sediment grain as reflected by its settling velocity depend on the volume, density, and maximum projection area of the grain (De Kruijf et al., 2021). Numerous experimental studies, therefore, characterize sediments by reporting volume and area values obtained using common measurement techniques (Blott and Pye, 2008; Bagheri et al., 2015). Approximations of volume and maximum projection area are typically based on the ellipsoidal model (longest diameter of ellipsoid and bounding box are parallel, Figure 1) that uses the axial lengths of the bounding box to estimate grain volume $\left(V = \frac{\pi}{6}.D_l.D_i.D_s\right)$ and maximum projection area $\left(A = \frac{\pi}{4}.D_l.D_i\right)$ (Wadell, 1932; Barrett, 1980).

3. Material and methods

3.1. Sediments and datasets used in this analysis

Skeletal carbonate grains include a variety of grain shapes that make them suitable for validating several measurement techniques. The tested sediment population is derived from a cool-water carbonate factory, and composed of the skeletal remains of red algae, bivalves, bryozoans, benthic foraminifers, echinoids, serpulids, and barnacles (same sediment as studied by Slootman et al., 2019). The solid density (i.e., mineral density excluding skeletal macro-porosity) is 2.0 to 3.5 mg.mm^{-3} (mean ± standard deviation = 2.7 ± 0.156 mg.mm^{-3}, Slootman et al., 2023).

Grains from a single carbonate sand population were used in the analysis, subsampled into three subsets. Subset A (n = 552) was used for micro-CT scanning (CT-GM). Subset B (n = 2,336) included 543 grains that were first measured using the caliper method (Caliper) and then analyzed using static image analysis on loose grains (SIA–Loose grain); all 2,336 grains were analyzed using static image analysis on thin sections (SIA–Thin section). Subset C (n = 4,338) was used for dynamic image analysis with the Microtrac MRB Camsizer P4 (DIA-Loose grain, Figure 2). Since all subsets originate from a single population, sediment composition and grain-size distribution throughout the analysis are uniform, thus ensuring a similar representation of the biogenic grain properties. Subsets were split into grain-size classes through dry sieving (Table 2). Analytical results are reported and compared by referring to these sieve grain-size classes.

3.2. Measurement and analytical methods

The micro-CT dataset is the dataset assumed to be the closest representation of true grain dimensions to which

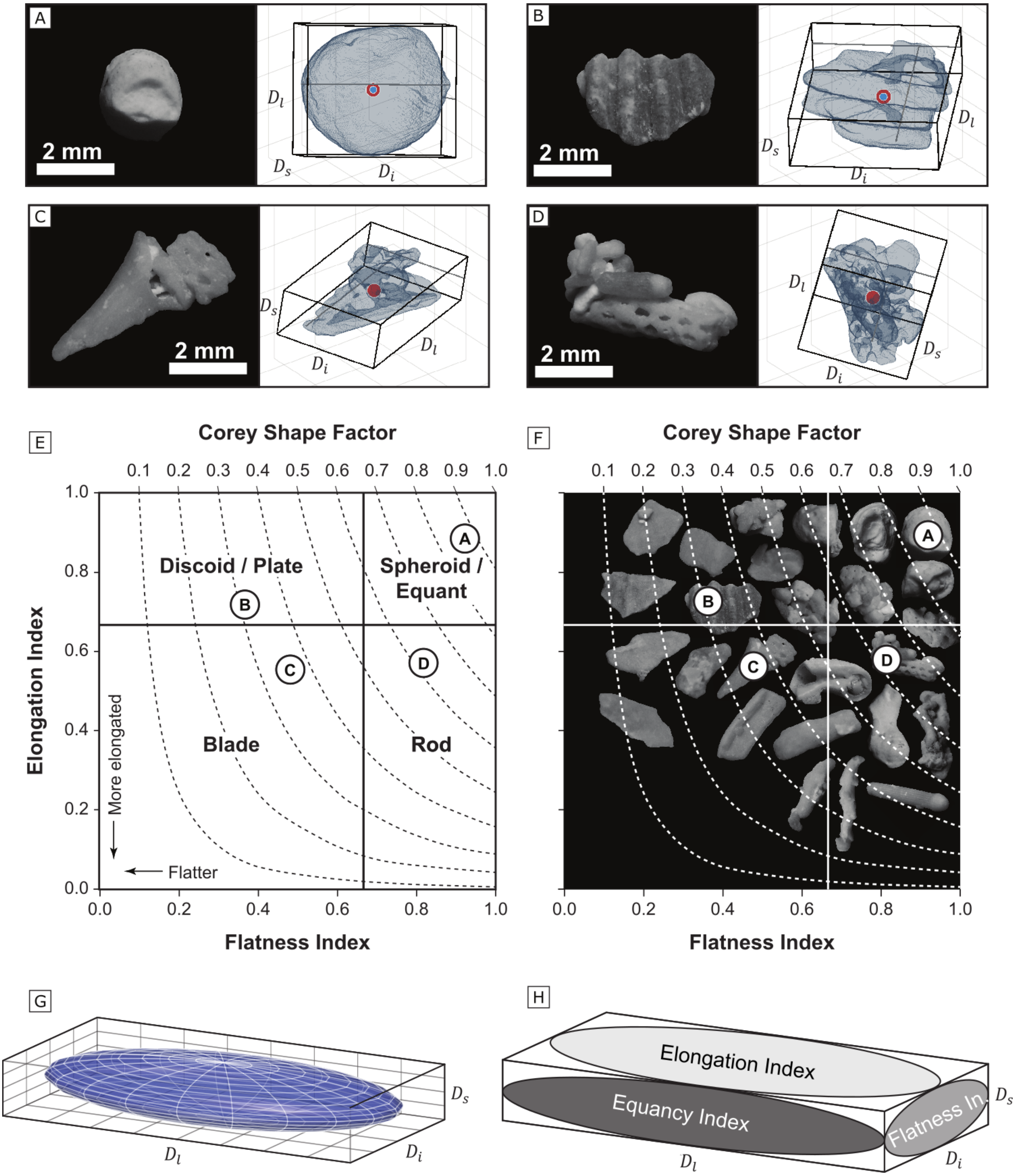

Figure 1 | (A-D) Examples of grain photographs (left) and digital models with maximum bounding box obtained with micro-CT. (E-F) Form classification in the Zingg (1935) diagram based on flatness and elongation. Corey shape factor isolines are displayed. Grains in A-D are identified in the diagram. (G) Bounding-box ellipsoid. Note that the longest axis of the grain is parallel to the longest dimension of the bounding box. (H) Indices of the ellipsoidal model (images modified from Slootman et al., 2023).

Calculated Grain Parameter	Computation
Dimensional Parameters	
Maximum Projection Area	$A = \frac{\pi}{4}.D_l.D_i$
Volume	$V = \frac{\pi}{6}.D_l.D_i.D_s$
Nominal Diameter	$D_n = \sqrt[3]{D_l.D_i.D_s}$
Equivalent Diameter	$D_{eq} = \sqrt[3]{\frac{6}{\pi}.V_{meas}}$
Shape Parameters	
Elongation	$El = D_i/D_l$
Flatness	$Fl = D_s/D_i$
Equancy	$Eq = D_s/D_l$
Corey Shape Fac	$CSF = D_s/\sqrt{D_l.D_i}$

Table 1 | Grain size and shape parameters and corresponding computations.

the results of other measurement techniques are compared. The maximum bounding-box ellipsoid (BBE) for each grain defines a 3D model that approximates its first-order morphology (Carlson et al., 2003; Cnudde and Boone, 2013; Houghton et al., 2024). Specifications of the reference dataset (micro-CT grain model), and the tested techniques: (i) micro-CT bounding-box ellipsoid, (ii) caliper measurement, (iii) static image analysis-loose grain, (iv) static image analysis-thin section, and (v) dynamic image analysis, are shown in Figure 2.

3.2.1. Reference model: Micro-computerized tomography

Micro-computerized tomography (micro-CT) was used to reconstruct the detailed three-dimensional spatial distribution of each grain to generate the reference model. Sieved grains were fixed into epoxy resin and scanned using

Technique	Abbreviation	Measured Particle Parameter	Number of Grains	Diagram
Standard Dataset				
A Micro-CT Grain Model	CT-GM	Grain Volume Grain Area	552	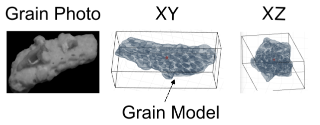
Approximation of Standard Dataset				
B Micro-CT Bounding-box Ellipsoid	CT-BBE	**Bounding Ellipsoid Dimensions** Long Diameter (D_l) Intermediate Diameter (D_i) Short Diameter (D_s)	552	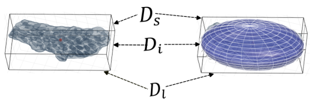
Tested Techniques				
C Caliper Measurement	Caliper	**Projection Axes** Long Diameter (D_l) Intermediate Diameter (D_i) Short Diameter (D_s)	543	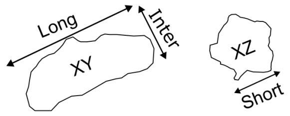
D Static Image Analysis Loose Grain	SIA-Loose grain	**Projection Axes** Long Diameter (D_l) = Major Axis Intermediate Diameter (D_i) = Minor Axis Short Diameter (D_s) (From Caliper meas.)	543	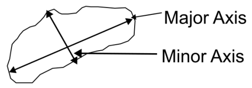
E Static Image Analysis Thin Section	SIA-Thin section	**Projection Axes** Major Axis Minor Axis	2,336	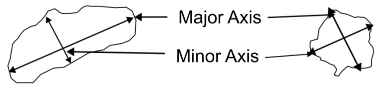
F Dynamic Image Analysis Loose Grain	DIA-Loose grain S1 DIA-Loose grain S2	**Projection Axes** Maximum Feret Diameter (XFeMax) Minimum Feret Diameter (XFeMin) Minimum Chord Diameter (Xcmin) Equivalent Circle Diameter (Xarea)	4,338	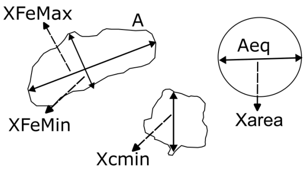

Figure 2 | Overview of grain size and shape measurement techniques and their outputs. The reference dataset consists of micro-CT scans (CT-GM), providing high-resolution 3D grain volumes and 2D projected areas. An ellipsoid approximation (CT-BBE) was computed from this reference dataset using standard equations for volume and maximum projection area (Table 1), based on the principal axes estimated from the grain model. These were compared to tested techniques, including caliper measurements, static image analysis (SIA) from loose grains and thin sections, and dynamic image analysis (DIA) from loose grains. SIA-Loose grain dimensions are based on the maximum projection area, while SIA-Thin section values depend on the sectioning plane. Two DIA-Loose grain variants estimate principal axes using: (S1) maximum Feret (XFeMax), minimum Feret (XFeMin), and minimum chord (XcMin); and (S2) XFeMax, equivalent circle diameter (XArea), and XcMin. DIA includes the equivalent circle diameter (Xarea), defined as the diameter of a circle with the same projected area (Aeq).

Sieve Size Range (mm)	Wentworth Size Class
>1.70	Very coarse (upper) sand and coarser
1.14 - 1.70	Very coarse (medial) sand
1.00 - 1.14	Very coarse (lower) sand
0.71 - 1.00	Coarse (upper) sand
0.5 - 0.71	Coarse (lower) sand

Table 2 | Sieve classes used.

a FEI Heliscan microCT (Thermo Fisher Scientific, Waltham, MA, USA) at the Center for Integrative Petroleum Research at King Fahd University in Dhahran, Saudi Arabia (see Slootman et al. (2023) for detailed analytical description). The accuracy of grain size measurement using micro-CT is constrained by voxel resolution (Payton et al., 2024). In this study, voxel resolution was 10×10×10 µm³, which is orders of magnitude larger than measured grains. Digital grain models contain between 344 and 50,735 voxels. A total of 552 grains were measured, ranging from 0.5 mm to 2.5 mm equivalent diameter (Table 1, Figure 3).

The micro-CT Grain Model dataset (CT-GM) contains the closest estimates of grain volume, as well as the maximum projection area obtained from the model of the grain by rotating it to every possible orientation in MATLAB (Figure 1). Subsequently, volume and maximum projection area were also approximated from the bounding-box ellipsoid (CT-BBE) constructed from the dimensions of the digital micro-CT grain models (Figure 2). Note that the longest diameter of the ellipsoid is parallel to the longest axis of the bounding box (Bagheri et al., 2015).

3.2.2. Caliper measurement

A digital caliper with an accuracy of 0.02 mm and resolution of 0.01 mm was used to measure the axes of grains following the projection area protocol of Bagheri et al. (2015). This protocol prescribes measurement of the long and intermediate axes on the maximum-area projection, and the short axis on the minimum-area projection of the grain (Figure 2C). This method does not require strict perpendicularity between the measured axes, as is the case

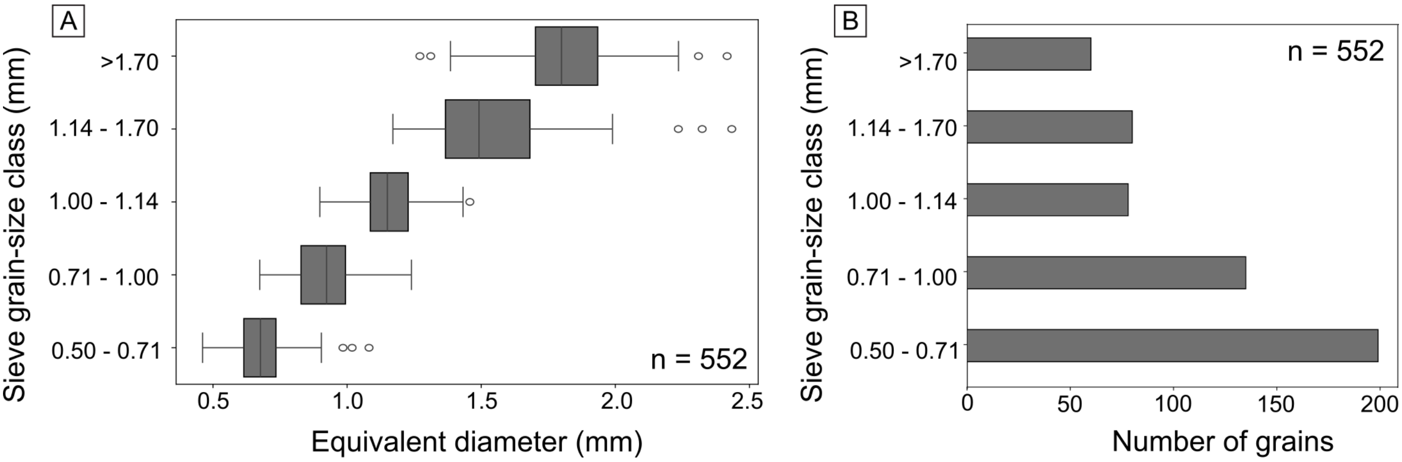

Figure 3 | (A) Distribution of equivalent diameters of grains measured using micro-CT. (B) Number of grains in each sieve grain-size class.

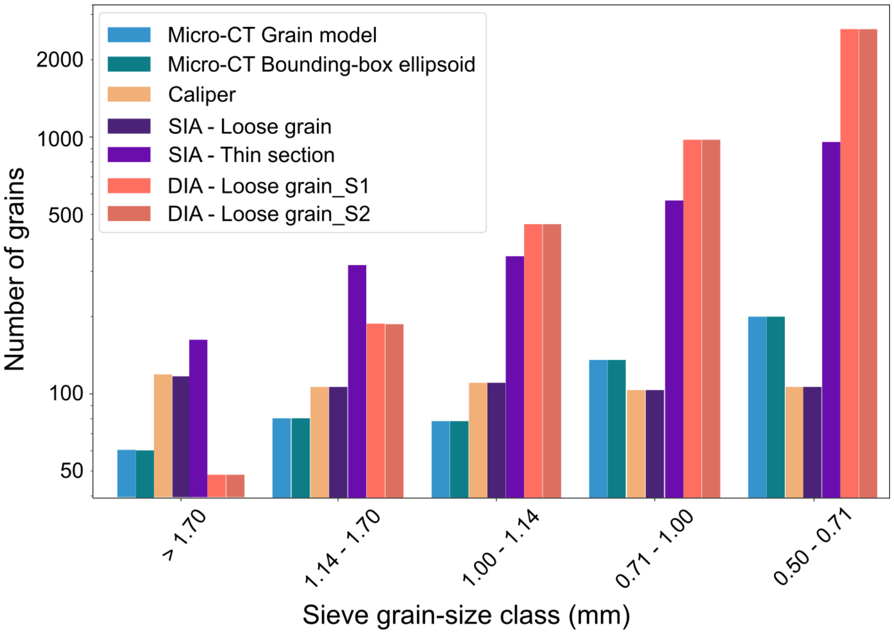

Figure 4 | Number of measured grains in each sieve grain-size class.

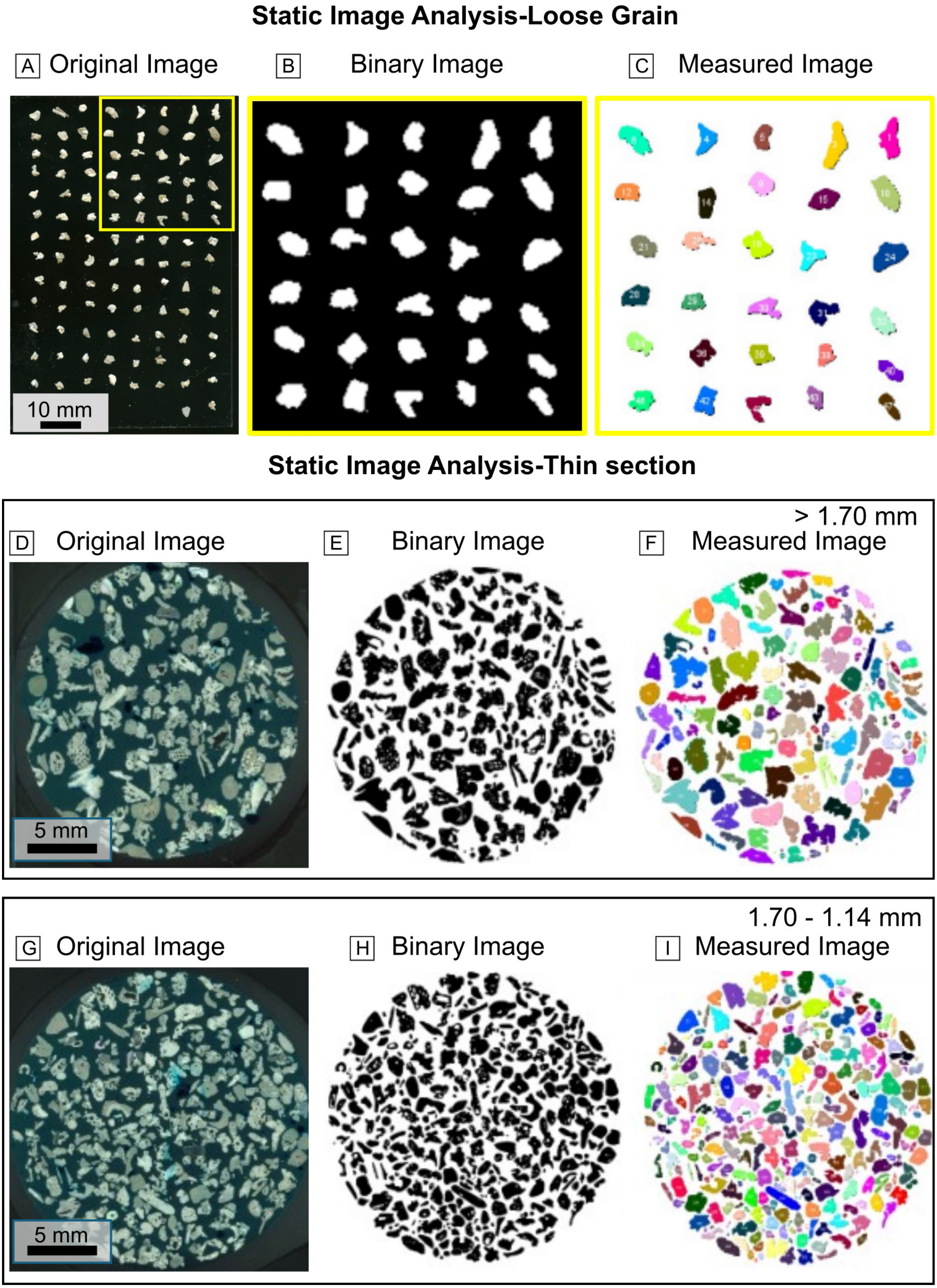

Figure 5 | Static image analysis workflow for loose grains (dataset SIA-Loose Grain). (A) Scanned image of the grains. (B) Binary image. (C) Labeled grains for class 1.14 to 1.70 mm. (D-I) Original, binary, and labeled image of the thin sections for sieve grain sizes >1.70 mm and 1.14 to 1.70 mm, respectively.

for the maximum bounding-box models (Krumbein, 1941a; Blott and Pye, 2008). Bagheri et al. (2015) recommend this non-perpendicularity to reduce operator-dependent errors. Caliper measurements (Caliper) were taken for at least 100 grains for each sieve grain-size class (Figure 4).

3.2.3. Static image analysis on loose grains

Image analysis of loose grains (SIA-Loose grain) was used to determine the major and minor axes of the maximum projection of the grains. The images were obtained with an Epson V850 flatbed scanner at 1200 dpi resolution and converted to binary images to optimize their identification and analysis (see methodology of Otsu, 1979, and Russ, 2006) (Figure 5). Binarization was achieved through pixel thresholding, where a cutoff intensity value was applied to distinguish grain pixels from the background. For each image, the pixel threshold range (mostly between 100 to 150 pixels in 8-bit grayscale) was determined individually by visual inspection to ensure complete grain capture without edge erosion and with minimal inclusion of artifacts. Pixels with intensities greater than or equal to the selected threshold were classified as grains (white), whereas those below the threshold were classified as background (black), resulting in a binary image. This binarization step enabled clear separation of grain boundaries and served as the foundation for subsequent morphological operations. Image morphological operations, including opening, closing, erosion, and dilation, were applied and tested for each image. A manual sensitivity analysis before and after these operations validated the process, ensuring that no real edges or pixels were lost during segmentation. Segmentation, morphological operation, and measurement were carried out using the image-analysis software ImageJ (Schneider et al., 2012). The obtained dimensional parameters were analyzed in Python to compute and visualize grain maximum projection areas, volumes, and shape descriptors.

Loose grains were arranged on a 50.8 mm (2400 pixels) by 76.2 mm (3600 pixels) glass plate to establish a non-touching, grid-like pattern (Figure 5A) to ensure the identification of individual grains. Grains are assumed to have rested with their maximum projection area facing downward. In this position, the long and intermediate axes were determined from the major axis and its perpendicular minor axis based on the best-fit ellipse on the 2D projection. The short axis, representing grain thickness, was measured separately using a digital caliper taken perpendicular to the maximum projection plane.

3.2.4. Static image analysis on thin sections

The methodology for static image analysis of thin sections (SIA–Thin Section) followed the same approach as that used for loose grains. However, instead of analyzing grains in a loose state, they were embedded in epoxy resin to prepare thin sections, with one section made for each sieve grain size class (Figure 5D–I). During preparation, grains were allowed to settle under the influence of gravity through the epoxy, promoting a range of grain orientations. Since static image analysis of thin sections yields only two-dimensional area measurements, this method will be considered separately in subsequent comparisons due to its inherent dimensional limitations.

3.2.5. Dynamic image analysis

Dynamic image analysis (DIA) was carried out using a Microtrac MRB (formerly Retsch Technology) Camsizer P4 (DIA; ISO 13322-2) at the University of Colorado at Boulder Chemical Sedimentology Lab. The particle analyzer uses a conveyor sample feeder system to pass loose grains through an imaging field. Two high-resolution digital cameras, one basic and one zoomed-in, that are backlit by a LED, with a measuring range between 0.02 and 30 mm in diameter, captured multiple images as the grains fell freely through air. Captured images were processed by the Camsizer software that generates shape and size distribution statistics (see Castro and Andronico, 2008; Buckland et al., 2021).

Two approaches (S1 and S2) were used to estimate the three principal dimensions of grain morphology. In the first method, the long, intermediate, and short axes were represented by the maximum Feret diameter (XFeMax), the minimum Feret diameter (XFeMin), and the minimum chord diameter (XcMin), respectively. The second method differed only in how the intermediate axis was represented: it used the equivalent circular diameter (XArea) in place of XFeMin, while retaining XFeMax and XcMin for the long and short axes, respectively (Figure 2). This second approach is commonly adopted in grain-size characterization studies (e.g., Castro and Andronico, 2008; see Buckland et al., 2021 for further parameter definitions).

4. Results

4.1. Volume-Area relationships

The long, intermediate, and short axes of grains were characterized using four measurement methods: Micro-CT Grain Model (CT-GM), caliper measurement (Caliper), static image analysis of loose grains (SIA–Loose grain), and dynamic image analysis of loose grains (DIA–Loose grain S1 and S2). Across all methods, the strongest positive correlation was consistently observed between the long and intermediate axes, while correlations involving the short axis were weaker (Figure 6).

Cumulative distribution functions (Figure 7) illustrate the volume and maximum projection area distributions for each measurement method. Caliper and SIA–Loose grain methods show similar distribution trends with minor differences. In contrast, more pronounced discrepancies are observed when comparing CT-GM with either the caliper or SIA methods, particularly in maximum projection area estimations.

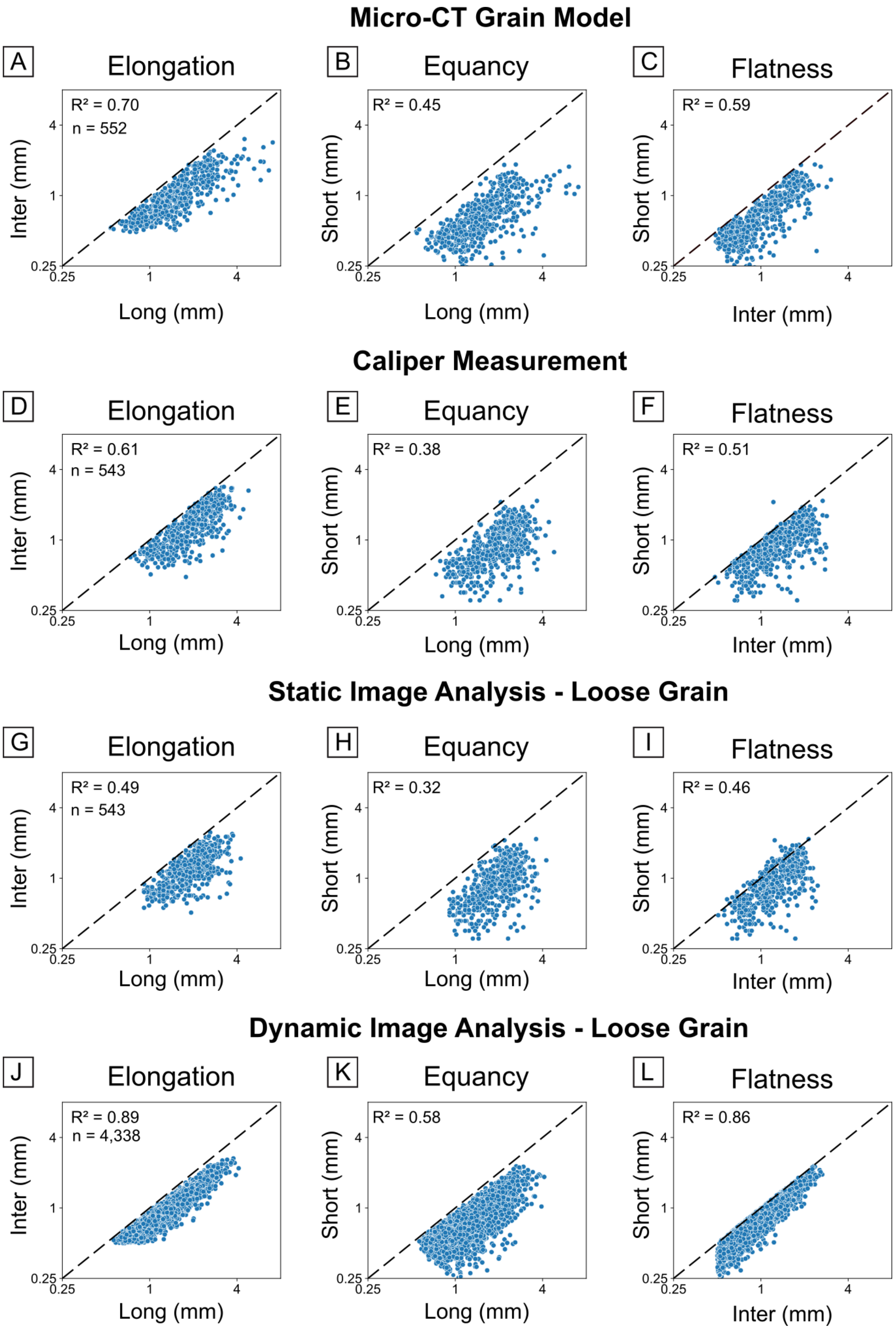

Figure 6 | Comparison of measured grain dimensions across four datasets, with each row representing one measurement method. Long, intermediate (Inter), and short axes are plotted against each other, and for each dataset, three plots display the principal shape parameters (Table 1). DIA-Loose Grain S1 is displayed here. Elongation is more pronounced than flatness, as indicated by the stronger positive correlation between the long and intermediate axes compared to the short axis correlations.

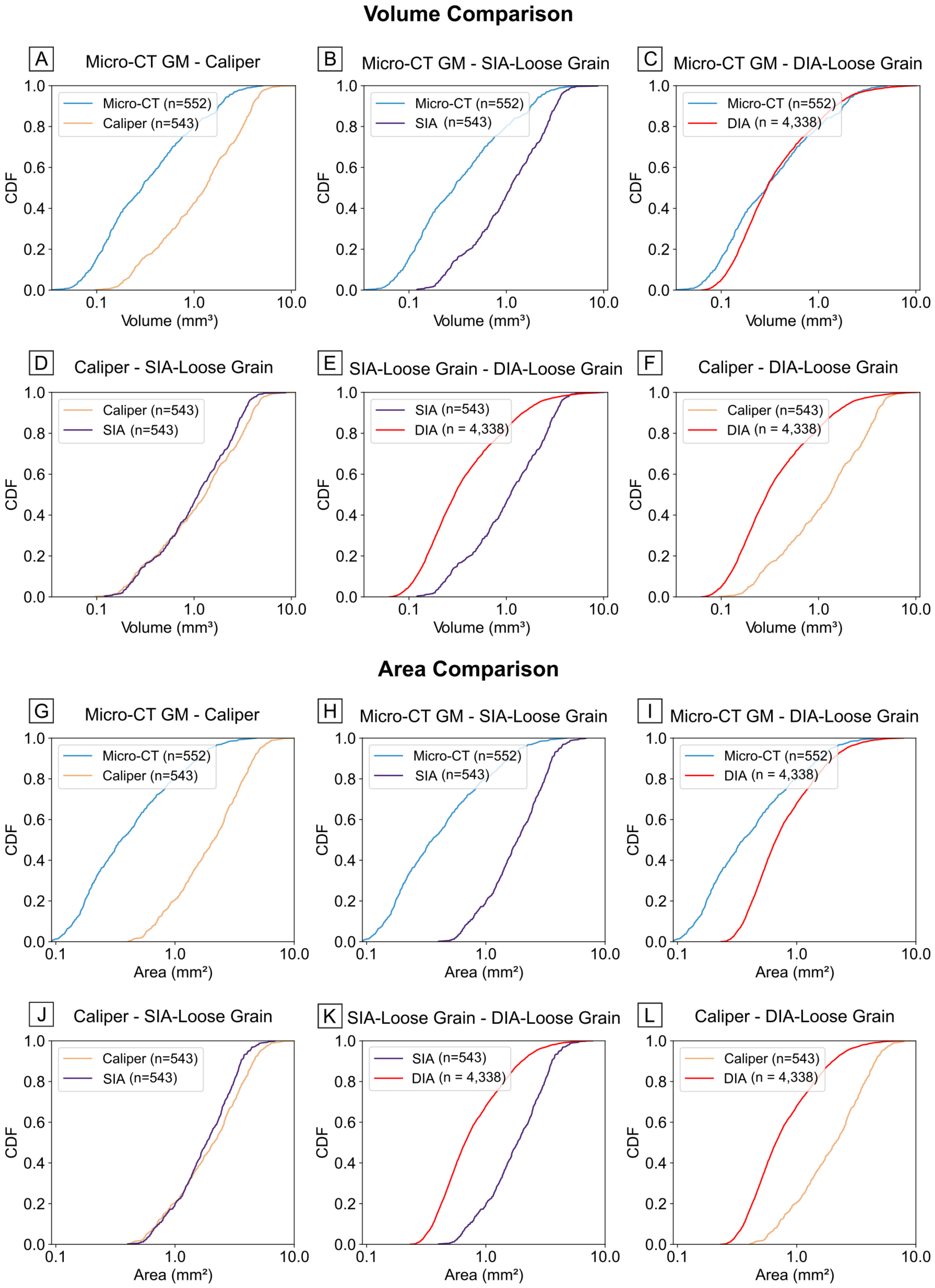

Figure 7 | Comparison of volume (A–F) and area (G–L) measurements using the different techniques. Cumulative distribution functions (CDFs) are shown. SIA refers to SIA-Loose grain analysis. DIA-Loose Grain S1 is displayed here.

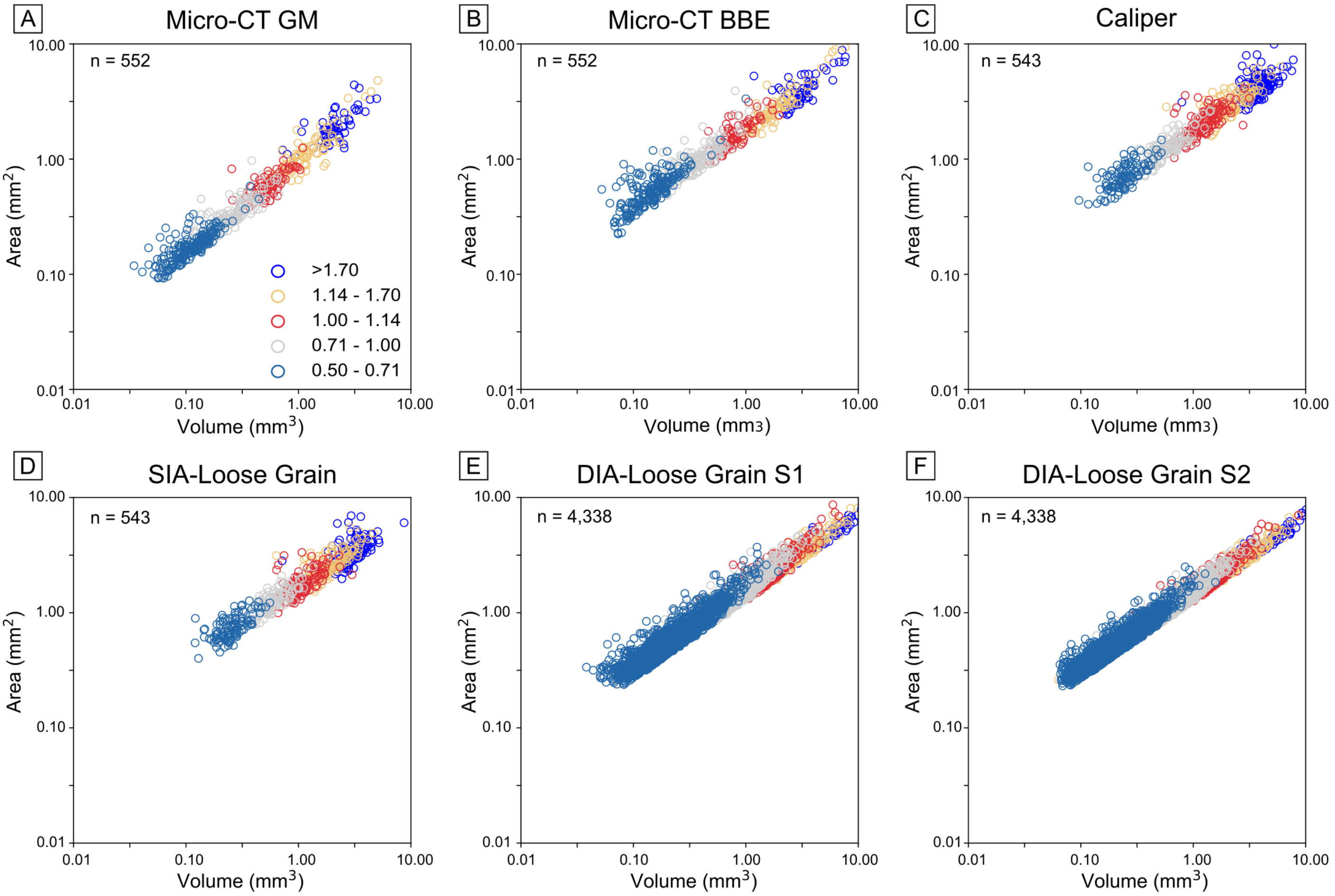

Figure 8 | Volume-Area ratio by grain-size class for each measurement method.

All methods exhibit a consistent trend in which area increases with volume. Data points cluster by grain size class, with some overlap between adjacent classes (Supplementary Figure S1). As shown in Figure 8, the CT-GM method displays the most compact distributions, while caliper measurements, SIA–Loose, and DIA–Loose methods exhibit greater variability.

A combined volume-area plot (Figure 9A) illustrates the comparative distributions across all measurement methods. While all datasets follow a broadly similar volume-area trend, notable differences exist in surface area estimates for equivalent volumes. The CT-GM consistently reports the lowest surface area, whereas the other methods, such as CT-BBE, caliper, and SIA-Loose grain, tend to overestimate the surface area. The difference in the volume-area trend is particularly pronounced in the CT-GM compared to methods that estimate dimensions using an ellipsoidal bounding box (SIA-Loose grain, caliper, and CT-BBE). When CT-GM is excluded, the regression lines for volume–area relationships among SIA–Loose, Caliper, and CT-BBE methods begin to diverge with increasing grain size. (Figure 9A). The CT-GM and DIA–Loose grain methods exhibit lower variability in volume and area measurements (Figures 9B, 9C). In contrast, CT-BBE consistently yields higher volume and area values and shows the broadest spread among all methods (Figure 9B and 9C).

4.2. Grain shape classification

The CT-GM results reveal a broad range of grain shapes, with a moderate dominance of rod- and discoid-like forms (Figure 10). Caliper measurements produce a similar distribution. In contrast, the SIA–Loose grain method yields a narrower shape range, with the highest proportion of rod-shaped grains among all methods. The DIA–Loose method predominantly classifies grains as spheroidal, accounting for over 80% of the results, with very few rods, discoids, or blades. When using the alternative classification criterion (representing the intermediate axis with XArea instead of XFeMax, see Figure 2), the DIA–Loose method identifies slightly more rod- and blade-shaped grains.

The CSF distributions for CT-GM and CT-BBE are identical because the parameters to compute CSF are identical. They are closely aligned with caliper measurements, displaying a moderately broad spread centered around intermediate values (Figure 10H). The SIA–Loose method shows a similar trend but with slightly greater dispersion. In contrast, the DIA–Loose method exhibits a sharp peak at high CSF values, indicating a tendency to overclassify grains as more spherical.

CSF values approaching one correspond to more spheroidal grains, whereas lower CSF values indicate more elongate or flatter forms (see Supplementary Figure S1).

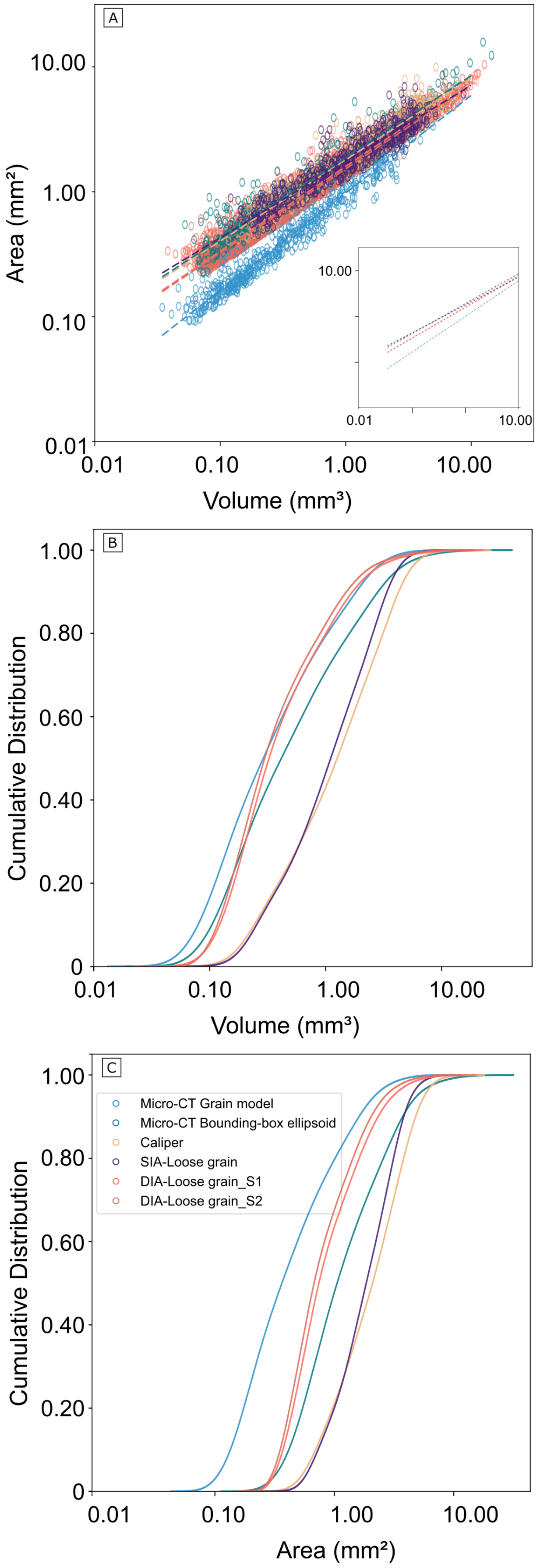

Figure 9 | (A) Combined volume-area plot comparing all measurement methods. Cumulative distribution functions for each method are shown for (B) volume and (C) area. All methods follow a similar trend, but area estimates vary for the same volumes. The micro-CT grain model (CT-GM) consistently measures the lowest surface area, while Micro-CT Bounding-box ellipsoid (CT-BBE) and other methods tend to overestimate the property.

These trends align with the shape classifications obtained in the Zingg diagram. While some variability exists in the volume–area relationships and shape categories across methods, the CSF distributions remain broadly consistent, with the exception of the DIA–Loose grain method, which tends to overestimate the degree of sphericity.

4.3. Comparison between thin section and loose grain image analysis

Static image analysis of thin sections (SIA–Thin section) produces major and minor axial measurements that are notably smaller than those obtained from loose grain static image analysis (SIA–Loose grain). This size reduction is attributed to the random orientations at which grains are sectioned during thin section preparation, often producing non-representative cross-sections that capture variable 2D slices of the grain (Figure 11A). In contrast, the SIA–Loose grain data exhibit a more organized distribution, with grain measurements clustering tightly within distinct size ranges across all grain size classes (Figure 11B). Such clear grouping is less apparent in the SIA–Thin section data.

4.4. Predicting the third dimension from two-dimensional data

A limitation of 2D grain measurements is that they cannot fully capture three-dimensional geometry, limiting the accurate characterization of grain shape. If it were possible to reliably infer 3D dimensions from 2D data, this would greatly advance our understanding of sediment properties and transport behavior. As a step toward addressing this limitation, linear regression analysis is employed to predict the short and intermediate grain axes using measurements from the micro-CT dataset (n=1,216). The models are derived from observed relationships among the long, intermediate, and short axes, and are expressed as follows:

$$\text{Short (Pred)} = 0.0247 + (0.0032 * \text{Long}) + (0.6014 * \text{Intermediate}) \qquad \text{(Equation 1)}$$

$$\text{Intermediate (Pred)} = 0.0782 + (0.155 * \text{Long}) + (0.9894 * \text{Short}) \qquad \text{(Equation 2)}$$

These equations provide a predictive framework for estimating grain dimensions from two known axes.

The Short (Pred) model yields a coefficient of determination of $R^2 = 0.78$, indicating a good overall fit in the initial dataset used for the regression model. However, prediction accuracy varies with grain size. Relative error tends to increase with larger grains (Figure 12), while smaller grains exhibit greater variability, with a wider spread of underpredicted values. The distribution of residuals was generally balanced, with both over- and underestimation occurring across the dataset (Figure 12B).

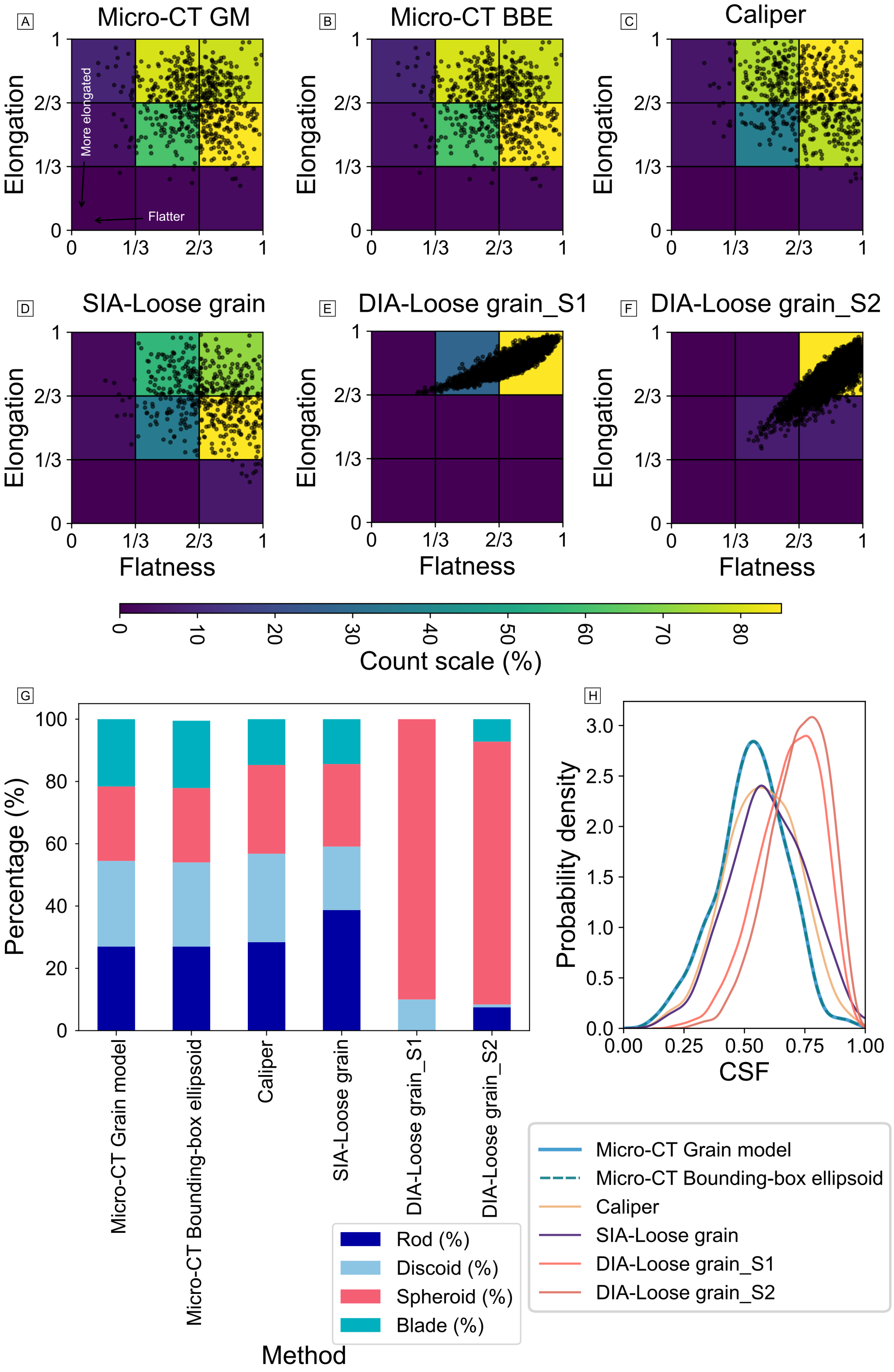

Figure 10 | (A-F) Zingg diagrams showing relative differences in grain shape classification across measurement techniques. (G) Qualitative distribution of grain shapes (Rod, Discoid, Spheroid, and Blade) from different grain measurement methods based on Zingg quadrant classification (Supplementary Figure 1). (H) Distribution of Corey Shape Factor (CSF) calculated from axial dimensions for each method.

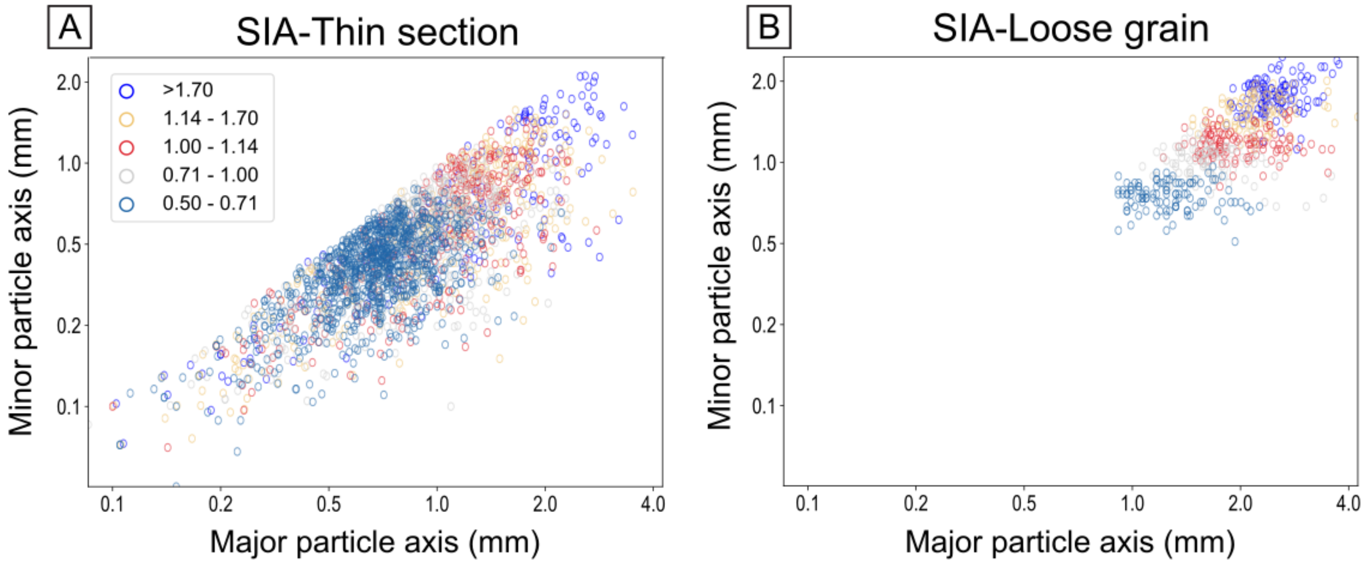

Figure 11 | Minor and major grain axis relationships grouped by grain-size classes for (A) thin section and (B) loose grain static image analysis.

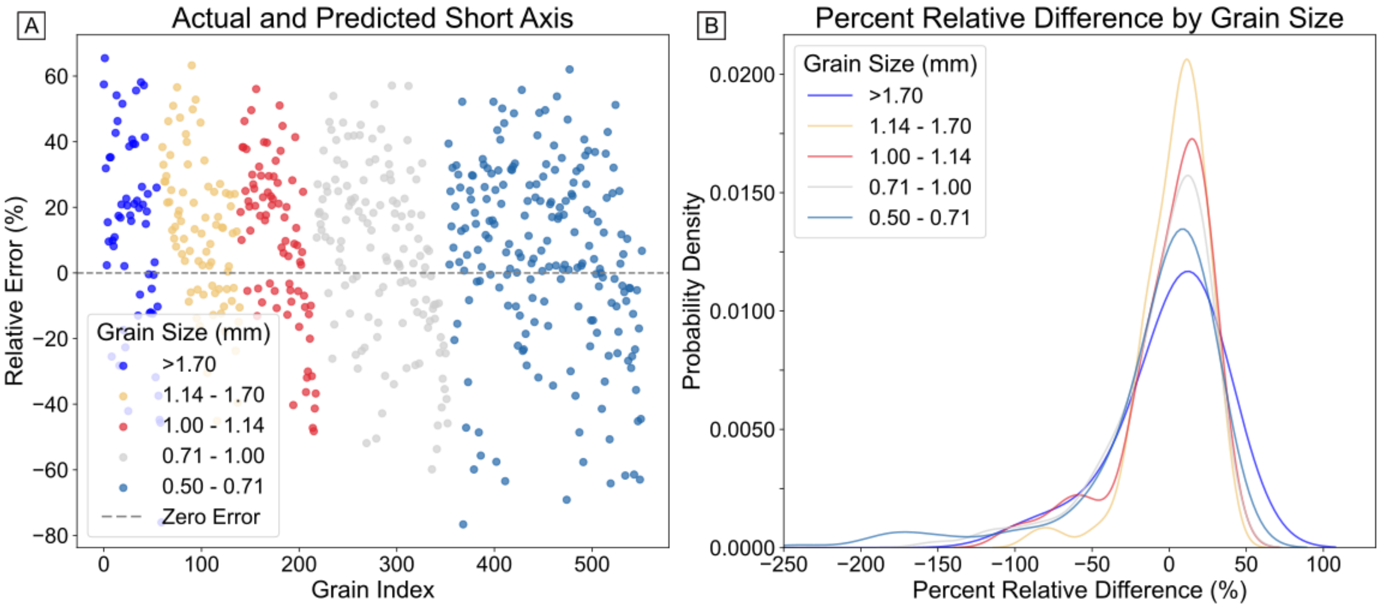

Figure 12 | (A) Differences between actual and predicted short-axis values, with each data point colored according to its grain size. (B) Density plot of the percentage difference between actual and predicted short-axis values, grouped by grain size. This plot illustrates the relative accuracy of the predicted short-axis values, with curves representing the distribution of percent differences for each grain size class.

Volumes calculated using predicted short-axis values (via Equation 1) show strong agreement with the reference volumes obtained from the CT-GM dataset. The distributions closely align with minimal spread (Figure 13), indicating that the regression model provides reliable volume estimates for this sediment population.

4.4.1. Model validation

To evaluate the robustness of the regression model, it was tested on another micro-CT dataset from the same sediment population (n = 1,125, Slootman et al., 2023, specifically using samples from their distal flume-floor deposits). Relative errors for predicted short-axis values were primarily confined within ±25% (Figures 14A and 14C), although absolute differences increased with grain size (Figure 14B). A Q–Q plot of the residuals for the tested population (Figure 14D) revealed a departure from normality, particularly in the lower tail, where large negative residuals indicate a tendency for underprediction. Despite this deviation, the model effectively captures key trends and offers overall estimates for similar sediment populations.

The regression model was also applied to thin-section data to evaluate its utility in predicting three-dimensional grain properties, including volume and surface area. Because thin sections provide only two-dimensional projections, we tested two assumptions regarding axis correspondence: (1) that the major and minor projections represent the long and intermediate axes, and (2) that

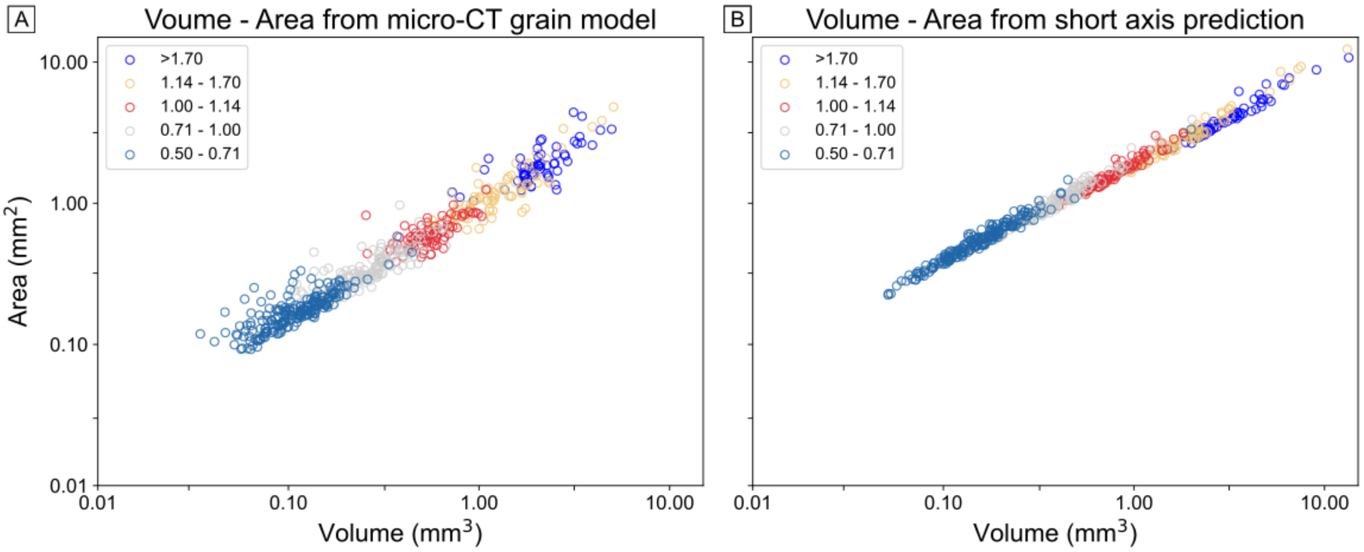

Figure 13 | Plot of volume against area grouped by grain size class for Micro-CT scan data with (A) actual measurements and (B) predicted short axis dimensions calculated using equation 1.

they represent the long and short axes (see Figures 1E–F and 11A). Under these assumptions, the remaining third axis was predicted using Equations 1 and 2. To assess the model's performance, the predicted area and volume distributions were compared with those from CT-GM (used to train the model) and caliper measurements (Figure 15). The results show that predicted volumes follow a similar trend to the reference dataset (Figure 15C and 15D), particularly for the volume–area relationship (Figure 15A and 15B).

5. Discussion

5.1. Variation in size and shape by measurement techniques

This study evaluates grain volume, area, and shape distributions as determined by caliper measurement, static image analysis (SIA), dynamic image analysis (DIA), and thin-section methods. Each technique is benchmarked against high-resolution micro-computed tomography (micro-CT), which serves as the reference standard due to its proven accuracy in capturing three-dimensional morphology (Houghton et al., 2024). This comparison is especially critical for irregular carbonate grains, whose complex geometries are often inadequately characterized by traditional techniques.

Spheroid grains consistently display the lowest surface area-to-volume ratios across all measurement techniques, whereas blade-shaped grains show the highest ratios. Rod-shaped and discoidal grains fall in between, with rods exhibiting slightly lower surface areas than discoids for equivalent volumes. These trends are evident in the CT-GM, SIA–Loose grain, and caliper datasets and reflect the expected geometric principle that spheres minimize surface area for a given volume (Osserman, 1978). DIA results, however, disproportionately classify grains as spheroids, a consequence of the assumptions embedded in its measurement algorithms.

Clustering and partial overlap of data points across size classes, particularly among larger grains, indicate that grain shape strongly influences volume–area relationships (Figure 8). This shape effect becomes more pronounced in coarser fractions. The impact of shape on volume is critical because it challenges the assumption, common in siliciclastic systems, that grain size alone reflects depositional energy, especially when grains deviate from idealized spheroidal forms (Kuenen & Migliorini, 1950).

In siliciclastic studies, grain size is frequently used as a proxy for depositional energy, predicated on the assumption that transported grains are primarily spheroidal and compositionally uniform (Kuenen & Migliorini, 1950). Under such conditions, one- and two-dimensional shape descriptors provide reliable estimates of grain behavior (Baba & Komar, 1981; Yordanova & Hohenegger, 2007). However, carbonate grains often exhibit non-equant shapes and heterogeneous density distributions. Consequently, two-dimensional descriptors are insufficient for accurately characterizing three-dimensional morphology in these systems (Su & Yan, 2019). For example, differences in how grain volume and area are estimated, especially between ellipsoidal based methods and actual 3D models, result in method-dependent discrepancies. These differences are quantitatively captured in the summary statistics (Table 3) and illustrated in Figures 6 through 10.

5.2. Accuracy and limitations of measurement techniques

Variability in grain-shape classification across methods underscores the sensitivity of morphological analysis to the chosen measurement technique. Each method has inherent strengths and limitations, which can significantly influence the accuracy of dimensional estimates and, by

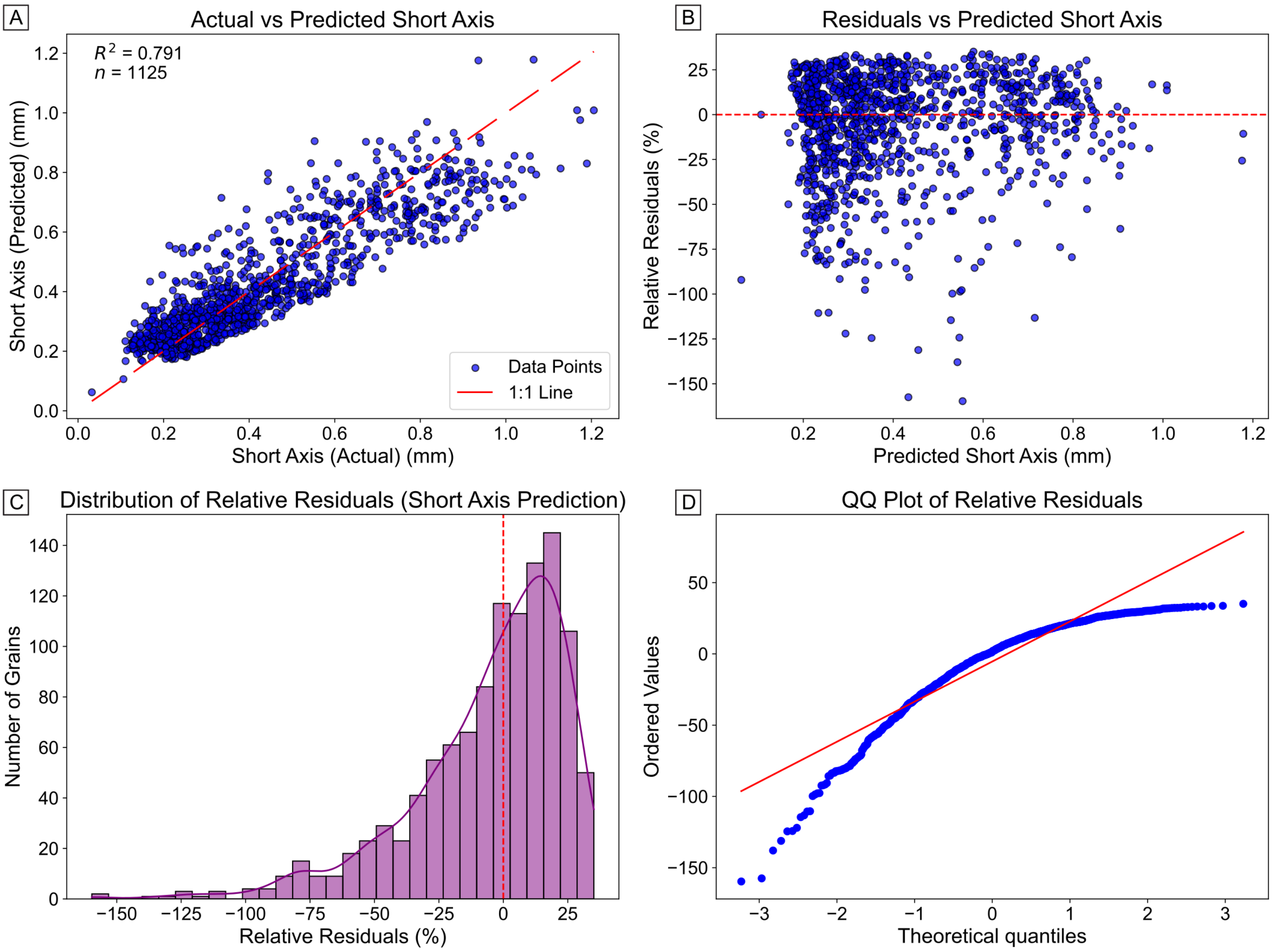

Figure 14 | (A) Actual versus predicted short-axis values, with the red dashed line indicating the 1:1 line and inset showing R2 and sample size (n). (B) Relative residuals (%) versus predicted short-axis, with the red dashed line indicating zero error. (C) Histogram showing left-skewed distribution of residuals, with most near zero. (D) Q–Q plot reveals non-normal residuals, especially in the lower tail, indicating more underestimates in the prediction for this test. Ordered values are the residuals ranked from smallest to largest.

extension, interpretations of grain behavior and depositional processes.

Volume and area estimates from static image analysis, caliper measurements, and ellipsoidal estimation using micro-CT data rely on bounding-box ellipsoid dimension approximations. In contrast, micro-CT grain models capture the true voxel-based geometry. As shown in Figure 9A, the disparity between these methods follows convergence at smaller grain sizes. This suggests that ellipsoidal approximations become increasingly inaccurate as grain complexity increases, especially for coarse grains. The CT-GM dataset exhibits the least scatter, reflecting its higher precision, whereas caliper measurements show greater variability due to inconsistencies in manual measurements.

Micro-CT offers highly accurate, voxel-based 3D reconstructions of grain morphology, providing detailed insight into internal structure and surface complexity. This makes it particularly valuable for characterizing irregular or composite grains. However, limitations include high acquisition costs, specialized software requirements, and computational demands for image segmentation and analysis, which hinder its widespread adoption.

Caliper-based measurements are constrained by their limited range and reliance on manual handling. Operator bias, particularly in aligning grains and identifying axis endpoints, can introduce significant errors, especially for non-equant grains (Blott & Pye, 2008; Bagheri et al., 2015). Variability in how baseline measurements are defined often leads to inconsistent shape classification compared to more objective techniques like micro-CT or SIA.

Static image analysis (SIA) is inherently limited by its two-dimensional nature, which restricts accurate capture of grain three-dimensional morphology. Segmentation challenges, such as grain edge erosion, artifact removal, and separating touching grains, can lead to the truncation or merging of grains. In thin sections, random cutting planes intersect grains in inconsistent orientations, often underestimating their true size and altering shape distribution (Cuzzi and Olson, 2017; van der Jagt et al., 2025). These limitations can skew estimates of porosity, permeability, or surface area. While specialized software has been developed to

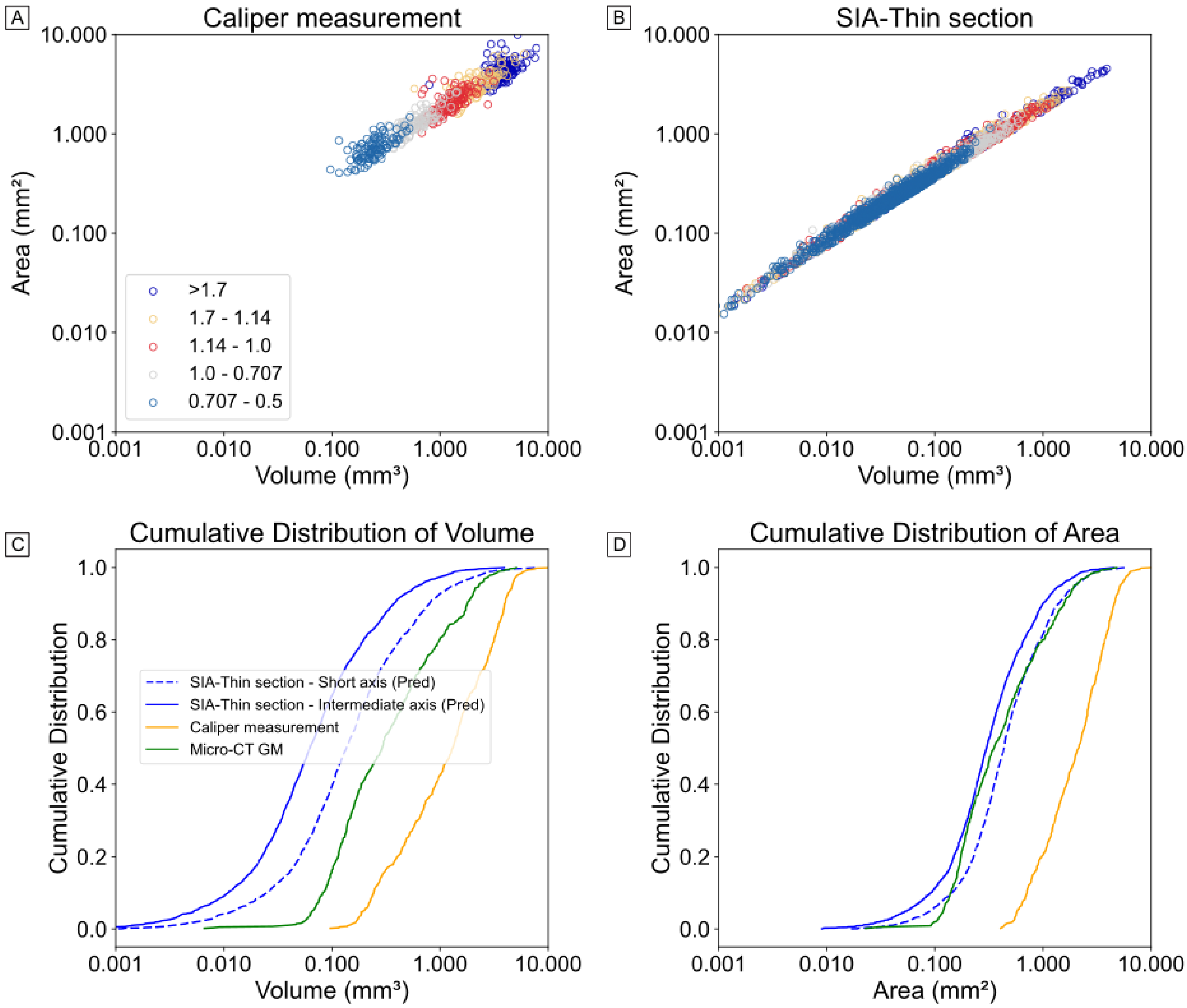

Figure 15 | (A - B) Area–volume relationships obtained from thin-section predictions with those from caliper measurements. The model-predicted volumes based on thin-section axes produce distributions that align with the caliper results, with the difference attributed to the errors incurred by using 2D measurements and sectioning bias, as opposed to a closer representation from the Micro-CT GM. (C – D) Volume and area distribution of the regression model used for estimating short and intermediate axes.

mitigate some of these issues (e.g., for siliciclastic grains), carbonate grain complexity warrants further method-specific correction protocols (Heilbronner & Barrett, 2013).

Dynamic image analysis (DIA) offers high-performance measurement capabilities, processing hundreds of images per second and capturing multiple shape metrics per grain (Microtrac MRB, 2020). While advantageous for large datasets, DIA assumes spherical geometry during analysis, leading to inaccuracies for irregularly shaped grains, as is particularly evident in this study. Measurement accuracy is also sensitive to calibration settings, image resolution, and grain size thresholds, which can introduce biases if not properly configured.

Despite inter-method differences in volume and area, the Corey Shape Factor (CSF) remains a consistent and robust descriptor across datasets (Supplementary Figure S1B). Its stability underscores its utility in quantifying grain morphology, particularly given its strong correlation with sediment settling behavior (De Kruijf et al., 2021; Slootman et al., 2023). However, as shown by the overestimation in DIA data, accurate CSF calculation still depends on precise axial dimension measurements. Importantly, while axial descriptors suffice for first-order shape estimation, accurate volume and area assessment requires a 3D representation of grain geometry.

Laser diffraction estimates grain size by analyzing light scattering patterns, which are interpreted under the assumption of spherical geometry (Malvern Panalytical, n.d.). This yields a volume-equivalent sphere diameter and works well for spherical grains. However, for irregular carbonate grains and volcaniclastics, this assumption can lead to substantial inaccuracies. In contrast, micro-CT directly measures true grain volume and geometry, enabling a more reliable calculation of nominal diameter (Figure 16) and providing critical data for refining shape-dependent grain transport dynamics models.

Parameter	Technique	Mean	Mode	Min	D10	D50	D90
CSF	CT-GM	0.529	0.127	0.127	0.340	0.533	0.711
	CT-BBE	0.529	0.127	0.127	0.340	0.533	0.711
	Caliper	0.574	0.585	0.160	0.382	0.578	0.765
	SIA - LG	0.602	0.557	0.153	0.391	0.594	0.813
	DIA - LG S1	0.686	0.197	0.197	0.505	0.701	0.844
	DIA - LG S2	0.723	0.267	0.267	0.556	0.735	0.872
Volume (mm^3)	CT-GM	0.634	0.120	0.034	0.086	0.293	1.796
	CT-BBE	1.011	0.052	0.052	0.111	0.408	2.758
	Caliper	1.760	0.730	0.096	0.243	1.304	3.963
	SIA - LG	1.475	0.280	0.120	0.254	1.105	3.209
	DIA - LG S1	0.708	0.038	0.038	0.126	0.321	1.666
	DIA - LG S2	0.633	0.063	0.063	0.120	0.295	1.473
Area (mm^2)	CT-GM	0.640	0.092	0.092	0.143	0.356	1.570
	CT-BBE	1.659	0.224	0.224	0.435	1.049	3.470
	Caliper	2.427	0.565	0.405	0.709	2.136	4.574
	SIA - LG	2.088	1.373	0.401	0.738	1.849	3.587
	DIA - LG S1	1.112	0.238	0.238	0.379	0.734	2.305
	DIA - LG S2	0.990	0.232	0.232	0.361	0.670	2.000

Table 3 | Grain volume, area, and CSF distribution statistics for all techniques and samples. (Caliper – Caliper Measurement, CT-GM – micro-CT Grain model, CT-BBE – Ellipsoidal estimation from CT data, SIA-LG – Static Image Analysis Loose grain, DIA-LG – Dynamic image analysis Loose grain (S1 – Scenario 1; S2 – Scenario 2 – see methods for scenario description).

5.3. Predictive modelling

In an ideal scenario, CT data gives the closest approximation of the grain volume and 3-axis dimensions, but this data is not common. Two-dimensional measurements are much more common (e.g., thin section, image data). In this study, we developed linear regression models to provide usable estimates for the third axis dimension (Figures 12, 13), which offers a practical, albeit biased, solution when complete 3D data is unavailable. Model accuracy is highest when based on measurements that closely match true grain dimensions, such as loose-grain imaging or micro-CT projections, and comparable to the sand population in this study. For thin-section measurements, however, the predicted third axis may reflect the inherent sectioning bias in the measured axes and should therefore be interpreted with this limitation in mind. Future work should more broadly validate these observations across various sedimentary environments and lithological types to establish the generalizability and robustness of these regression models.

Model prediction accuracy declines with increasing grain size (Figure 12A), possibly due to the increasing complexity and irregularity of larger grains (Komar & Reimers, 1978; Baba & Komar, 1981; Lui et al., 2015). This trend is also evident in static image-derived estimates of the short axis (Figure 15). Such predictive models are particularly valuable for thin-section or image-based datasets, where only two orthogonal projections of grain dimensions are available (Figure 2).

To test the applicability of the predictive models beyond the original dataset, we applied them to two independent datasets representing distinct sediment populations. The first dataset, from Alcérreca et al. (2013), contains 1,557 measurements of carbonate grains, including oolites, mollusk fragments, and coral detritus, collected from 58 coastal sites along the Yucatán Peninsula. The second, from Smith and Cheung (2003), includes 998 measurements of grain axes from calcareous sand samples collected in Oahu, Hawaii. Figures 17 and 18 illustrate the model's performance across these datasets, validating its use in tropical carbonate settings.

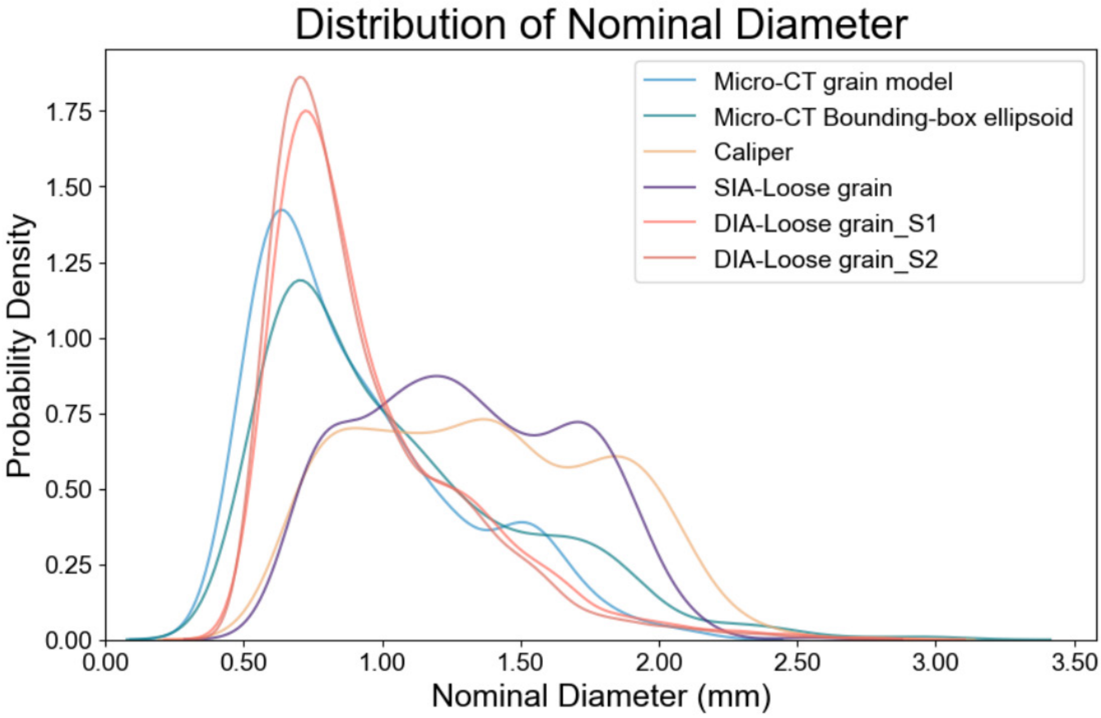

Figure 16 | Distribution of nominal diameters for grains measured using various methods.

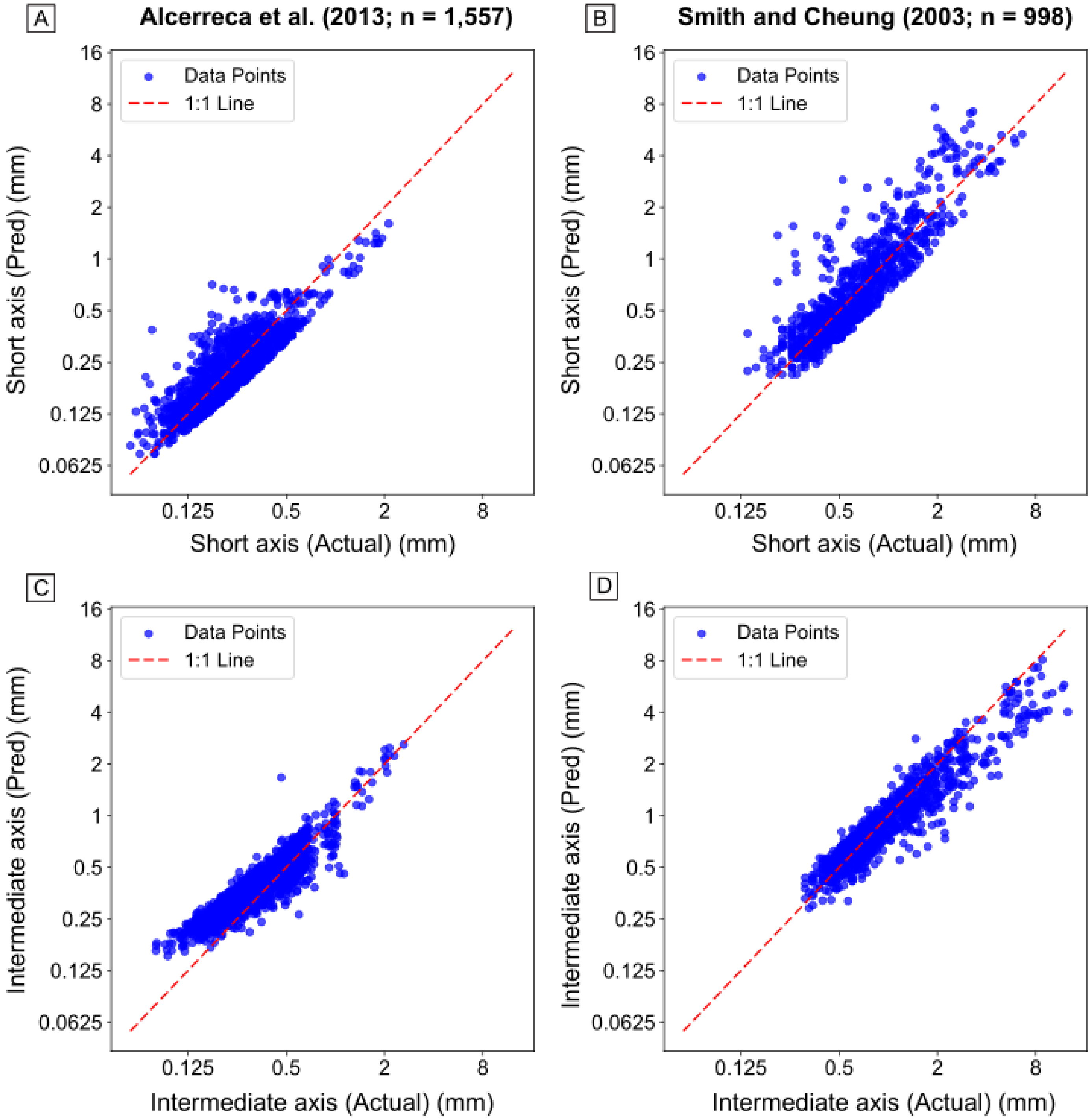

Equation 1 - Short (Pred) = 0.0247 + (0.0032 × Long) + (0.6014 × Inter)
Equation 2 - Inter (Pred) = 0.0782 + (0.155 × Long) + (0.9894 × Short)

Figure 17 | Comparison of predicted and actual values for Short and Intermediate dimensions based on equations derived from the micro-CT dataset in this study tested on datasets of Alcérreca et al. (2013) and Smith and Cheung (2003).

For the Alcérreca et al. (2013) dataset, predicted and actual dimensions align closely, with cumulative distribution curves showing minimal deviation and prediction accuracies of 78.83% for the short axis and 72.88% for the intermediate axis. Similarly, predictions using the Smith and Cheung (2003) data achieved 71.80% and 82.56% accuracy for short and intermediate axes, respectively. These results demonstrate that, at first approximation, the model's capacity to capture dimensional trends across different carbonate sediment populations.

5.3.1. Assumptions and limitations of the predictive model

Linear regression assumes linearity, independence, normality, and homoscedasticity of residuals (Kutner et al., 2005). Scatter plots (Figure 6) suggest a generally linear relationship among grain axes in the training data, but Q-Q plots reveal slight deviations from normality in the test data, particularly at the distribution tails (Figure 14D). This non-linearity contributes to increasing prediction errors at

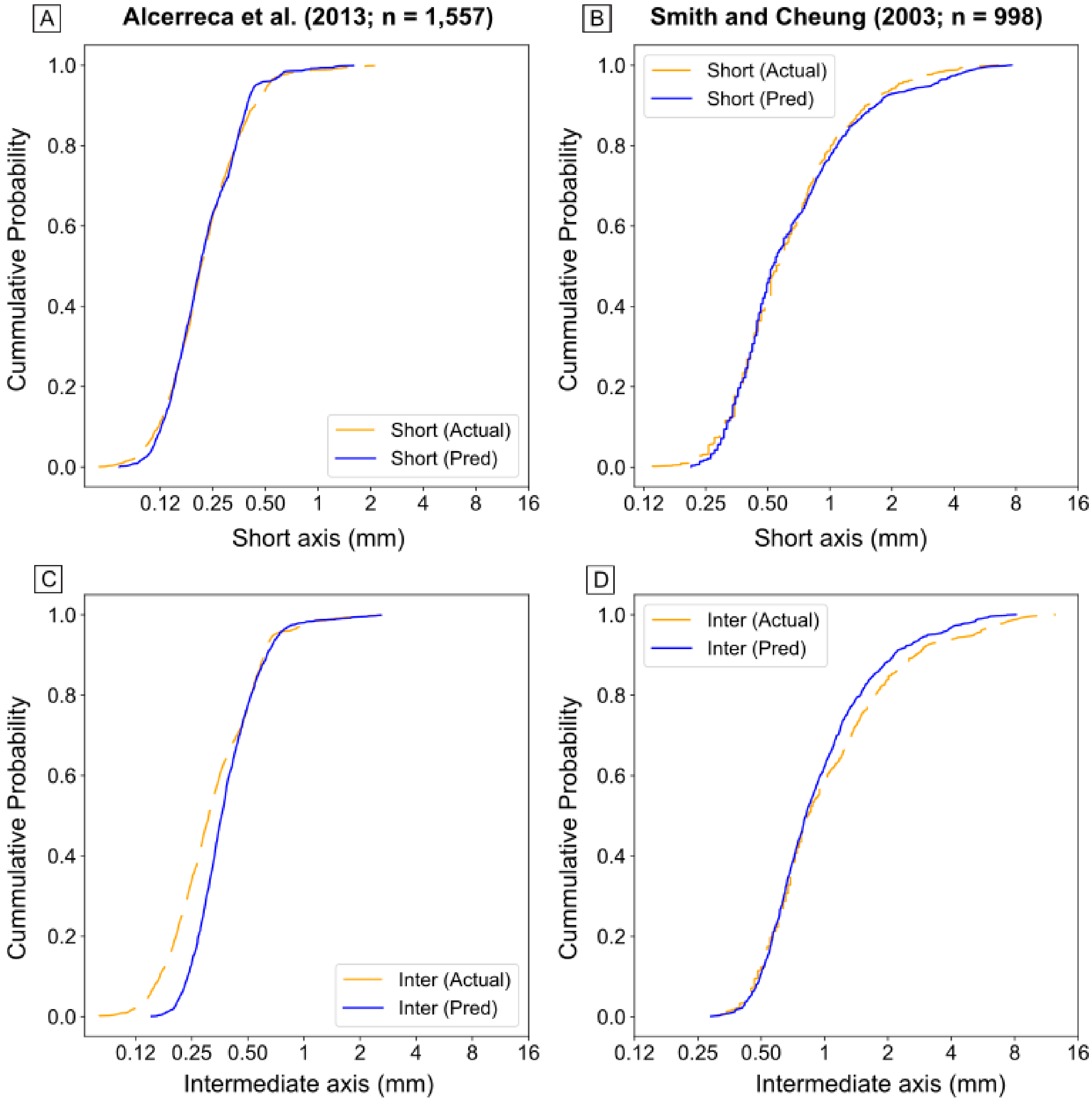

Figure 18 | Comparison of predicted and actual values for Short and Intermediate (Inter) dimensions based on equations derived from the micro-CT dataset in this study tested on Alcérreca et al. (2013) and Smith and Cheung, (2003) datasets.

both ends of the grain size spectrum, indicating that the model performs best for grains of intermediate size.

Although the models show promising results, deviations between predicted and actual values suggest that grain-size-specific variability, especially at larger sizes, introduces heteroscedasticity (i.e., the prediction errors are not uniformly distributed but tend to increase with grain size). Attempts to fit separate regression models by grain size class led to overfitting (Supplementary Figure S2), prompting the selection of a single, unified model that balances generality with predictive accuracy.

To assess the potential benefit of non-linear models, we compared linear regression with a second-degree polynomial fit. The polynomial model yielded a marginally lower mean squared error (MSE = 0.0197) compared to the linear model (MSE = 0.0204). Given the negligible improvement, the linear model was retained for its simplicity and interpretability. However, further data transformations (e.g., log or power transformations) could be explored to improve future predictive performance, though they are beyond the scope of this study.

Despite some limitations, the regression model demonstrates satisfactory accuracy, as evidenced by its performance across multiple datasets. Its consistency in capturing cumulative trends reinforces its utility for estimating grain dimensions when only partial data are available. However, caution is warranted when applying the model to sediments with substantially different grain-shape distributions, as prediction accuracy may decline. Dataset-specific calibration remains essential for ensuring reliable use in varied geological settings.

6. Conclusions

This study presents a comprehensive comparison of grain measurement techniques, evaluating their effectiveness in characterizing volume, surface area, and morphology of irregularly shaped grains. Among all methods, micro-computed tomography (Micro-CT) provides the most reliable and detailed representation of grain geometry, particularly in defining volume–area relationships. Despite its accuracy, Micro-CT's high cost and limited accessibility restrict its widespread application in routine sedimentological analysis.

Caliper-based measurements, though accessible and widely used, tend to mis-estimate grain length and suffer from operator-dependent variability, introducing bias in shape classification. Static image analysis, particularly on thin sections, underrepresents grain size due to random orientations and limited two-dimensional perspectives. Dynamic image analysis offers rapid and repeatable measurements; however, its assumption of spherical grain geometry limits its accuracy for shape determination in non-equant grains. Despite these differences, Corey Shape Factor (CSF) distributions remain broadly consistent across most techniques, except DIA, suggesting that axial dimensions are reasonably captured, while estimates of two- and three-dimensional properties remain more sensitive to the chosen method.

The linear regression model developed for estimating the third grain dimension from two-dimensional data demonstrates promising predictive capability. However, its applicability across varied sedimentological contexts remains uncertain and requires further validation. Future work may benefit from incorporating machine learning approaches to enhance model generalizability, particularly in datasets with diverse grain shapes and textural complexity.

Acknowledgements

We gratefully acknowledge the support of the American Chemical Society Petroleum Research Fund (ACS-PRF) and the Colorado School of Mines Geology Center of Research Excellence, whose funding made this research possible. Thank you to Prof. Cheung, K. F., Dr. Alcerreca, J. C., and Dr. Slootman, A., for sharing their datasets. We also appreciate Dr. Arnoud Slootman and the anonymous reviewers for their valuable feedback and suggestions, which improved the quality of this manuscript.

Author contribution

Chibuzor David Nworie: Conceptualization, Data curation, Formal Analysis, Investigation, Methodology, Software, Validation, Visualization, Writing – original draft, Writing – review & editing. Zane R. Jobe: Conceptualization, Funding acquisition, Project administration, Supervision, Validation, Writing – review & editing.

Data availability

Data used in this work is available at https://zenodo.org/records/14294942.

Conflict of interest

The authors declare that they have no known competing personal relationships or financial interests that could have appeared to influence the work reported in this paper.

References

Alcérreca, J. C., Silva, R., & Mendoza, E. (2013). Simple settling velocity formula for calcareous sand. Journal of Hydraulic Research, 51(2), 215–219. https://doi.org/10.1080/00221686.2012.753645.

Al-Rousan, T. (2004). Characterization of aggregate shape properties using a computer automated system [Ph.D. dissertation, Texas A&M University]. ProQuest Dissertations and Theses Global.

Al-Rousan, T., Masad, E., Tutumluer, E., & Pan, T. (2007). Evaluation of image analysis techniques for quantifying aggregate shape characteristics. Construction and Building Materials, 21(5), 978–990. https://doi.org/10.1016/j.conbuildmat.2006.03.005

Askaripour, M., Saeidi, A., Mercier-Langevin, P., & Rouleau, A. (2022). A review on relationship between texture characteristic and mechanical properties of rock. Geotechnics, 2(1), 262–296. https://doi.org/10.3390/geotechnics2010012

Baba, J., & Komar, P. D. (1981). Measurements and analysis of settling velocities of natural quartz sand grains. Journal of Sedimentary Research, 51(2), 631–640. https://doi.org/10.2110/jsr.51.631

Bagheri, G. H., Bonadonna, C., Manzella, I., & Vonlanthen, P. (2015). On the characterization of size and shape of irregular particles. Powder Technology, 270, 141–153. https://doi.org/10.1016/j.powtec.2014.10.015.

Bagheri, G., & Bonadonna, C. (2016). On the drag of freely falling non-spherical particles. Powder Technology, 301, 526–544. https://doi.org/10.1016/j.powtec.2016.06.015

Barrett, P. J. (1980). The shape of rock particles: A critical review. Sedimentology, 27(3), 291–303. https://doi.org/10.1111/j.1365-3091.1980.tb01179.x

Blott, S. J., & Pye, K. (2008). Particle shape: A review and new methods of characterization and classification. Sedimentology, 55(1), 31–63. https://doi.org/10.1111/j.1365-3091.2007.00892.x

Bowman, E. T., Soga, K., & Drummond, W. (2001). Particle shape characterisation using Fourier descriptor analysis. Géotechnique, 51(6), 545–554. https://doi.org/10.1680/geot.2001.51.6.545

Braithwaite, C. J. R. (1973). Settling behaviour related to sieve analysis of skeletal sands. Sedimentology, 20(2), 251–262. https://doi.org/10.1111/j.1365-3091.1973.tb02048.x

Buckland, H. M., Saxy, J., Roche, M., Meredith, P., Rust, A. C., Cashman, K. V., & Engwell, S. L. (2021). Measuring the size of non-spherical particles and the implications for grain size analysis in volcanology. Journal of Volcanology and Geothermal Research, 415, 107257. https://doi.org/10.1016/j.jvolgeores.2021.107257

Buscombe, D., Rubin, D. M., & Warrick, J. A. (2010). A universal approximation of grain size from images of noncohesive sediment. Journal of Geophysical Research: Earth Surface, 115, F02015. https://doi.org/10.1029/2009JF001477

Carlson, W. D., Rowe, T., Ketcham, R. A., & Colbert, M. W. (2003). Applications of high-resolution X-ray computed tomography in petrology, meteoritics, and palaeontology. Geological Society, London, Special Publications, 215(1), 7–22. https://doi.org/10.1144/GSL.SP.2003.215.01.02

Cassel, M., Lavé, J., Recking, A., Malavoi, J-R., Piégay, H. (2021). Bedload transport in rivers, size matters but so does shape. Scientific Reports, 11, 508. https://doi.org/10.1038/s41598-020-79930-7

Castro, M. D. L., & Andronico, D. (2008). Operazioni di base per la misura della distribuzione granulometrica di particelle vulcaniche tramite il CAMSIZER. Istituto Nazionale di Geofisica e Vulcanologia, Catania.

Clark, M. W. (1981). Quantitative shape analysis: A review. Mathematical Geology, 13(4), 303–320. https://doi.org/10.1007/BF01031516

Clift, R., & Gauvin, W. H. (1971). Motion of entrained particles in gas streams. Canadian Journal of Chemical Engineering, 49(4), 439–448. https://doi.org/10.1002/cjce.5450490403

Cnudde, V., & Boone, M. N. (2013). High-resolution X-ray computed tomography in geosciences: A review of the current technology and applications. Earth-Science Reviews, 123, 1–17. https://doi.org/10.1016/j.earscirev.2013.04.003

Corey, A. T. (1949). Influence of shape on the fall velocity of sand grains. Hydraulic Laboratory Report No. 21. Colorado Agricultural and Mechanical College, Fort Collins, CO.

Cuttler, M. V., Lowe, R. J., Falter, J. L., & Buscombe, D. (2017). Estimating the settling velocity of bioclastic sediment using common grain-size analysis techniques. Sedimentology, 64(4), 987–1004. https://doi.org/10.1111/sed.12338

Cuzzi, J. N., & Olson, D. M. (2017). Recovering 3D particle size distributions from 2D sections. Meteoritics & Planetary Science, 52(3), 532–545. https://doi.org/10.1111/maps.12812

De Kruijf, M., Slootman, A., de Boer, R. A., & Reijmer, J. J. G. (2021). On the settling of marine carbonate grains: Review and challenges. Earth-Science Reviews, 217, 103532. https://doi.org/10.1016/j.earscirev.2021.103532

Flemming, B. W. (2017). Particle shape-controlled sorting and transport behaviour of mixed siliciclastic/bioclastic sediments in a mesotidal lagoon, South Africa. Geo-Marine Letters, 37(4), 397 - 410. https://doi.org/10.1007/s00367-016-0457-3

Folk, R. L., & Robles, R. (1964). Carbonate sands of Isla Perez, Alacran reef complex, Yucatan. Journal of Geology, 72(3), 255–292. https://doi.org/10.1086/626986

Ford, M. R., & Kench, P. S. (2012). The durability of bioclastic sediments and implications for coral reef deposit formation. Sedimentology, 59(3), 830–842. https://doi.org/10.1111/j.1365-3091.2011.01281.x

Ghoddousi, P., Shirzadi Javid, A. A., & Sobhani, J. (2014). Effects of particle packing density on the stability and rheology of self-consolidating concrete containing mineral admixtures. Construction and Building Materials, 53, 102–109. https://doi.org/10.1016/j.conbuildmat.2013.11.076

Gibbs, R. J., Matthews, M. D., & Link, D. A. (1971). The relationship between sphere size and settling velocity. Journal of Sedimentary Research, 41(1), 7–18. https://doi.org/10.1306/74D721D0-2B21-11D7-8648000102C1865D

Griffiths, J. C. (1967). Scientific method in analysis of sediments (508 pp.). McGraw-Hill.

Hawie, N., Covault, J. A., & Sylvester, Z. (2019). Grain-size and discharge controls on submarine-fan depositional patterns from forward stratigraphic models. Frontiers in Earth Science, 7, 334. https://doi.org/10.3389/feart.2019.00334

Heilbronner, R., & Barrett, S. (2013). Image analysis in earth sciences: Microstructures and textures of earth materials (Vol. 129). Springer. https://doi.org/10.1007/978-3-642-10343-8

Hohenegger, J. (2006). The importance of symbiont-bearing benthic foraminifera for West Pacific carbonate beach environments. Marine Micropaleontology, 61(1–3), 4–39. https://doi.org/10.1016/j.marmicro.2006.05.007

Houghton, J. E., Behnsen, J., Duller, R. A., Nichols, T. E., & Worden, R. H. (2024). Particle size analysis: A comparison of laboratory-based techniques and their application to geoscience. Sedimentary Geology, 464, 106607. https://doi.org/10.1016/j.sedgeo.2024.106607

Jorry, S. J., Hasler, C. A., & Davaud, E. (2006). Hydrodynamic behaviour of Nummulites: Implications for depositional models. Facies, 52(2), 221–232. https://doi.org/10.1007/s10347-005-0035-z

Kench, P. S., & McLean, R. F. (1996). Hydraulic characteristics of bioclastic deposits: New possibilities for environmental interpretation using settling velocity fractions. Sedimentology, 43(3), 561–573. https://doi.org/10.1046/j.1365-3091.1996.d01-23.x

Knowlton, N., Brainard, R. E., Fisher, R., Moews, M., Plaisance, L., & Caley, M. J. (2010). Coral reef biodiversity. In A. D. McIntyre (Ed.), Life in the world's oceans: Diversity, distribution, and abundance (Chapter 4). Wiley-Blackwell. https://doi.org/10.1002/9781444325508.ch4

Komar, P. D., & Cui, B. (1984). The analysis of grain-size measurements by sieving and settling-tube techniques. Journal of Sedimentary Petrology, 54(2), 603–614. https://doi.org/10.1306/212F8481-2B24-11D7-8648000102C1865D

Komar, P. D., & Reimers, C. E. (1978). Grain shape effects on settling rates. Journal of Geology, 86(2), 193–209. https://doi.org/10.1086/649674

Krumbein, W. C. (1941a). Measurement and geological significance of shape and roundness of sedimentary particles. Journal of Sedimentary Research, 11(2), 64–72. https://doi.org/10.1306/D42690F3-2B26-11D7-8648000102C1865D

Krumbein, W. C. (1941b). The effects of abrasion on the size, shape, and roundness of rock fragments. The Journal of Geology, 49(5), 482–520. https://doi.org/10.1086/624985

Krumbein, W. C. (1942). Settling-velocity and flume-behavior of non-spherical particles. EOS, Transactions American Geophysical Union, 23(2), 621–633. https://doi.org/10.1029/TR023i002p00621

Kuenen, P. H., & Migliorini, C. I. (1950). Turbidity currents as a cause of graded bedding. Journal of Geology, 58(2), 91–127. https://doi.org/10.1086/625710.

Kutner, M. H., Nachtsheim, C., Neter, J., & Li, W. (2005). Applied linear statistical models (5th ed.). McGraw-Hill.

Laugié, M., Michel, J., Pohl, A., Poli, E., & Borgomano, J. (2019). Global distribution of modern shallow-water marine carbonate factories: A spatial model based on environmental parameters. Scientific Reports, 9, 16432. https://doi.org/10.1038/s41598-019-52821-2

Le Goff, J., Recouvreur, A., Reijmer, J. J. G., Mulder, T., Ducassou, E., Perelló, M. C., Hanquiez, V., Gillet, H., Cavailhes, T., & Fabregas, N. (2021). Linking carbonate sediment transfer to seafloor morphology: Insights from Exuma Valley, the Bahamas. Sedimentology, 68(2), 609–638. https://doi.org/10.1111/sed.12794

Le Roux, J. P. (1997). Comparison of sphericity indices as related to the hydraulic equivalence of settling grains. Journal of Sedimentary Research, 67(3), 527–530. https://doi.org/10.1306/D42685BD-2B26-11D7-8648000102C1865D

Lokier, S. W., & Fiorini, F. (2016). Temporal evolution of a carbonate coastal system, Abu Dhabi, United Arab Emirates. Marine Geology, 381, 102–113. https://doi.org/10.1016/j.margeo.2016.09.001

Maiklem, W. R. (1968). Some hydraulic properties of bioclastic carbonate grains. Sedimentology, 10(2), 101–109. 10.1111/j.1365-3091.1968.tb01102.x

Malvern Panalytical. (n.d.). Laser diffraction (LD). In Laser diffraction particle size analysis. Retrieved September 1, 2025, from https://www.malvernpanalytical.com/en/products/technology/light-scattering/laser-diffraction

Maroof, M. A., Mahboubi, A., Noorzad, A., & Safi, Y. (2020). A new approach to particle shape classification of granular materials. Transportation Geotechnics, 22, 100296. https://doi.org/10.1016/j.trgeo.2019.100296

Microtrac MRB. (2020). Microtrac particle characterization technical brochure. https://www.metrohm.com/content/dam/metrohm/en_au/documents/Microtrac_brochure_mrb_overview_en.pdf

Mohr, H., Draper, S., Cheng, L., & White, D. J. (2016). Predicting the rate of scour beneath subsea pipelines in marine sediments under steady flow conditions. Coastal Engineering, 110, 111–126. https://doi.org/10.1016/j.coastaleng.2015.12.010

Morgan, K. M., & Kench, P. S. (2014). A detrital sediment budget of a Maldivian reef platform. Geomorphology, 222, 122–131. https://doi.org/10.1016/j.geomorph.2014.02.013

Morgan, K. M., & Kench, P. S. (2016). Reef to island sediment connections on a Maldivian carbonate platform: Using benthic ecology and biosedimentary depositional facies to examine island-building potential. Earth Surface Processes and Landforms, 41(13), 1815–1825. https://doi.org/10.1002/esp.3946

Mulder, T., & Alexander, J. (2001). The physical character of subaqueous sedimentary density flows and their deposits. Sedimentology, 48(2), 269–299. https://doi.org/10.1046/j.1365-3091.2001.00360.x

Murff, J. D. (1987). Pile capacity in calcareous sands: State of the art. Journal of Geotechnical Engineering, 113(5), 490–507. https://doi.org/10.1061/(ASCE)0733-9410(1987)113:5(490)

Oakey, R. J., Green, M., Carling, P. A., Lee, M. W., Sear, D. A., & Warburton, J. (2005). Grain-shape analysis—A new method for determining representative particle shapes for populations of natural grains. Journal of Sedimentary Research, 75(6), 1065–1073. https://doi.org/10.2110/jsr.2005.079

Osserman, R. (1978). The isoperimetric inequality. Bulletin of the American Mathematical Society, 84(6), 1182–1238. https://doi.org/10.1090/S0002-9904-1978-14553-4

Otsu, N. (1979). A threshold selection method from gray-level histograms. IEEE Transactions on Systems, Man, and Cybernetics, 9(1), 62–66. https://doi.org/10.1109/TSMC.1979.4310076

Patchigolla, K., & Wilkinson, D. (2009). Crystal shape characterization of dry samples using microscopic and dynamic image analysis. Particle and Particle Systems Characterization, 26(4), 171–178. https://doi.org/10.1002/ppsc.200700030

Payros, A., & Pujalte, V. (2008). Calciclastic submarine fans: An integrated overview. Earth-Science Reviews, 86(1–4), 203–246. https://doi.org/10.1016/j.earscirev.2007.09.001

Payton, R. L., Chiarella, D., & Kingdon, A. (2022). The influence of grain shape and size on the relationship between porosity and permeability in sandstone: A digital approach. Scientific Reports, 12(1), 7531. https://doi.org/10.1038/s41598-022-11365-8

Payton, R. L., Chiarella, D., & Kingdon, A. (2024). An introduction for non-experts on using X-ray micro computed tomography as a tool for pore scale digital subsurface characterisation of siliciclastic materials. Sedimentologika, 2(2), e22.1367. https://doi.org/10.57035/journals/sdk.2024.e22.1367

Pettijohn, F. J. (1957). Sedimentary rocks (2nd ed.). Harper and Row.

Pilkey, O. H., Morton, R. W., & Lutemauer, J. (1967). The carbonate fraction of beach and dune sands. Sedimentology, 8(4), 311–327. https://doi.org/10.1111/j.1365-3091.1967.tb01330.x

Playton, T. E., Kerans, C., & Gamero-Diaz, H. (2010). Carbonate slopes. In N. P. James & R. W. Dalrymple (Eds.), Facies models 4 (pp. 449–476). Geological Association of Canada.

Playton, T. E., & Kerans, C. (2018). Architecture and genesis of prograding deep boundstone margins and debris-dominated carbonate slopes: Examples from the Permian Capitan Formation, Southern Guadalupe Mountains, West Texas. Sedimentary Geology, 370, 15–41. https://doi.org/10.1016/j.sedgeo.2017.12.021

Reijmer, J. J. G. (2021). Marine carbonate factories: Review and update. Sedimentology, 68(5), 1729–1796. https://doi.org/10.1111/sed.12878

Reijmer, J. J. G., Palmieri, P., & Groen, R. (2012). Compositional variations in calciturbidites and calcidebrites in response to sea-level fluctuations (Exuma Sound, Bahamas). Facies, 58, 493–507. https://doi.org/10.1007/s10347-011-0291-z

Riazi, A., & Türker, U. (2019). The drag coefficient and settling velocity of natural sediment particles. Computational Particle Mechanics, 6(3), 427–437. https://doi.org/10.1007/s40571-019-00223-6

Riazi, A., Vila-Concejo, A., Salles, T., & Türker, U. (2020). Improved drag coefficient and settling velocity for carbonate sands. Scientific Reports, 10(1), 9465. https://doi.org/10.1038/s41598-020-65741-3

Russ, J. C. (2006). The image processing handbook (5th ed.). CRC Press.

Schlager, W. (2003). Benthic carbonate factories of the Phanerozoic. International Journal of Earth Sciences, 92, 445–464. https://doi.org/10.1007/s00531-003-0327-x

Schneider, C. A., Rasband, W. S., & Eliceiri, K. W. (2012). NIH Image to ImageJ: 25 years of image analysis. Nature Methods, 9(7), 671–675. https://doi.org/10.1038/nmeth.2089.

Shen, Y., Feng, Z., Qi, W., Ma, Y., & Liu, H. (2019). Sedimentary characteristics of coral mud in the South China Sea during the reclamation process. Geo-Marine Letters, 39(5), 417–425. https://doi.org/10.1007/s00367-019-00600-3

Slootman, A., De Boer, P. L., Cartigny, M. J. B., Samankassou, E., & Moscariello, A. (2019). Evolution of a carbonate delta generated by gateway-funneling of episodic currents. Sedimentology, 66(4), 1302–1340. https://doi.org/10.1111/sed.12585

Slootman, A., De Kruijf, M., Glatz, G., Eggenhuisen, J. T., Zühlke, R., & Reijmer, J. (2023). Shape‐dependent settling velocity of skeletal carbonate grains: Implications for calciturbidites. Sedimentology, 70(6), 1683-1722. https://doi.org/10.1111/sed.13103

Smith, D. A., & Cheung, K. F. (2003). Settling characteristics of calcareous sand. Journal of Hydraulic Engineering, 129(6), 479–483. https://doi.org/10.1061/(ASCE)0733-9429(2003)129:6(479)

Stokes, G. G. (1851). On the effect of the internal friction of fluids on the motion of pendulums. Transactions of the Cambridge Philosophical Society, 9, 8.

Su, D., & Yan, W. M. (2019). Prediction of 3D size and shape descriptors of irregular granular particles from projected 2D images. Acta Geotechnica, 15, 1–23. https://doi.org/10.1007/s11440-019-00845-3

Sun, R., Xiao, H., & Sun, H. (2017). Realistic representation of grain shapes in CFD–DEM simulations of sediment transport with a bonded-sphere approach. Advances in Water Resources, 107, 421–438. https://doi.org/10.1016/j.advwatres.2017.04.015

van der Jagt, T., Vittorietti, M., Sedighiani, K., Bos, C., & Jongbloed, G. (2025). Estimation of 3D grain size distributions from 2D sections in real and simulated microstructures. Computational Materials Science, 256, 113949. https://doi.org/10.1016/j.commatsci.2025.113949

Van Hateren, J. A. V., Buuren, U. V., Arens, S. M., Balen, R. T. V., & Prins, M. A. (2020). Identifying sediment transport mechanisms from grain size–shape distributions, applied to aeolian sediments. Earth Surface Dynamics, 8(2), 527–553. https://doi.org/10.5194/esurf-8-527-2020

Wadell, H. (1932). Volume, shape, and roundness of rock particles. The Journal of Geology, 40(5), 443–451. https://doi.org/10.1086/623964

Walsh, D. E. (1988). A study of factors suspected of influencing the settling velocity of fine gold particles. University of Alaska Mineral Industry Research Laboratory.

Wang, Y., Zhou, L., Wu, Y., & Yang, Q. (2018). New simple correlation formula for the drag coefficient of calcareous sand particles of highly irregular shape. Powder Technology, 326, 379–392. https://doi.org/10.1016/j.powtec.2017.12.004

Wentworth, C. K. (1922). A scale of grade and class terms for clastic sediments. The Journal of Geology, 30(5), 377–392. http://www.jstor.org/stable/30063207

Worden, R. H., Armitage, P. J., Butcher, A. R., Churchill, J. M., Csoma, A. E., Hollis, C., Lander, R. H., & Omma, J. E. (2018). Petroleum reservoir quality prediction: Overview and contrasting approaches from sandstone and carbonate communities. Geological Society, London, Special Publications, 435(1), 1–31. https://doi.org/10.1144/SP435.21

Yordanova, E. K., & Hohenegger, J. (2007). Studies on settling, traction and entrainment of larger benthic foraminiferal tests: Implications for accumulation in shallow marine sediments. Sedimentology, 54(6), 1273–1306. https://doi.org/10.1111/j.1365-3091.2007.00881.x

Zhang, Z., Lan, X., Wen, G., Long, Q., & Yang, X. (2021). An experimental study on the particle size and shape distribution of coal drill cuttings by dynamic image analysis. Geofluids, 2021, 5588248. https://doi.org/10.1155/2021/5588248

Zingg, T. (1935). Beiträge zur Schotteranalyse. Schweizerische Mineralogische und Petrographische Mitteilungen, 15, 39–140. https://doi.org/10.3929/ethz-a-000103455

How to cite: Nworie, C. D., & Jobe, Z. R. (2025). Size and shape of carbonate grains: A comparison of measurement techniques. Sedimentologika, 3(1), 1-24. https://doi.org/10.57035/journals/sdk.2025.e31.1742